POLITECNICO DI TORINO

DIPARTIMENTO DI INGEGNERIA MECCANICA E AEROSPAZIALE
(DIMEAS)

Master's Degree in Biomedical Engineering

Assessing the robustness of the muscle synergies decomposition algorithm.

Supervisors
Prof. Gabriella Olmo
Prof. Paolo Bonato

Candidate
Letizia Viscogliosi

TORINO, October 2020

Abstract

The theory of "Muscle Synergies" has been formulated in the last few decades to have a better understanding of the optimization strategies applied by the Central Nervous System (CNS) in the control of the activation and coordination of the many muscles involved in any voluntary movement. The synergies can be considered as patterns of co-activation corresponding to the activity of few muscles: having to control a number of these modules lower than the actual number of muscles involved, the computational cost of every task is significantly reduced.

The synergies are modeled as a time-invariant profile of activation across muscles, activated by a time-varying coefficient. Summing the individual synergies, after having scaled them by their coefficient, the profile of muscle activation should be faithfully reconstructed. Different algorithms have been used in literature to extract the synergies from the sEMG data, in this study the Non-Negative Matrix Factorization (NNMF) decomposition algorithm was analyzed. The NNMF algorithm operates a data projection from a n-dimensional space to a lower k-dimensional space, where n is the number of channels considered and k the basis vectors, representing the synergies.

The focus of this thesis is analyzing the changes in the final factorization performed by the NNMF algorithm when one or more input channels are removed. During real data collection loss of channels can occur frequently due to bad quality of the recording. Having a different number of channels, it would not be possible to compare synergies obtained from signals collected from the same muscles, both for different subjects and for the same subject multiple times.

To approach the problem, sEMG data were synthesized, obtaining them from the linear combination of a simulated set of synergies, and an increasing number of channels was removed from the original signals. The performances of the NNMF

algorithm were evaluated comparing its outputs, i.e. synergies weights W and temporal coefficients H, for the starting signals where all the channels were still present and the signals with a decreasing number of channels. The metrics used for the comparison of the weights W and the temporal coefficients H were, respectively, the Cosine Similarity (CS) and the Correlation Coefficient (CC).

The analysis of the results of the various simulation performed pointed out that losing a limited number of channels does not compromise the ability of the NNMF algorithm to detect the same synergies and to reconstruct in a satisfying way the original signals, as long as not all the strategic channels or all the peculiar ones for a certain synergy are lost.

To test the algorithm in conditions as close as possible to the physiological ones, data from a gait analysis was simulated replicating the averaged EMG activity from 25 muscles during a single cycle of over-ground locomotion that could be found in literature. Also with this set of data the performances of the algorithm were good and the original synergies were preserved even when an high number of channels was removed.

Contents

List of Tables

List of Figures

Summary

The analysis of muscle synergies have a growing number of clinical application, mostly in the field of rehabilitation and in the study of neurological pathologies. The theory behind them provides a better understanding of the optimization strategies applied by the Central Nervous System. Muscle Synergies can be defined as patterns of co-activation of muscles, and can be modeled as time-invariant profile of activation across muscles, activated by a time-varying coefficient.
The most common algorithm for the extraction of muscle synergies is the Non-Negative Matrix Factorization Algorithm. This thesis focused on analyzing the performances of this algorithm when one or more input channels are lost.

This thesis is composed by four chapters:

1. **Muscular System Physiology and sEMG recording**: The anatomy of the muscular system, with a focus on the skeletal muscle, and the physiology behind the mechanism of contraction is explained, to have a better understanding of the principles behind the generation and propagation of the EMG signal. In the second part, the different ways to record EMG signal are explained, with a focus on the acquisition process and on the noise sources.

2. **Muscle Synergies**: the control theory behind the concept of muscle synergies is explained. In the state of the art part, a short evolution of application of this theory in experimental and clinical works is presented. Then, the process for the extraction of synergies is explained, focusing on the Non-Negative Matrix Factorization algorithm.

3. **Material and methods**: the practical steps to perform to extract muscle synergies from sEMG signals are presented, and the methods needed to analyze the performances of the NNMF algorithm. Then, the plan and methods applied in the four categories of simulations that were performed in the work for this thesis are presented, with a focus on a method for the simulation of sEMG signals.

4. **Simulations results and discussion**: The results of the four simulations are presented and analyzed.

5. **Conclusions**: An outline of the work done and the results obtained from this thesis.

Chapter 1

Muscular System Physiology and sEMG recording

1.1 Basic principles of the Muscular System

The muscular system is an organ system whose main function is the body movement, achieved in cooperation with the skeleton and the joints. The muscles composing the muscular system are also responsible for stability and posture control, production of heat, protection of the underlying organs and blood circulation.
Muscle cells are excitable, they respond to electrical stimuli, the Action Potential, delivered through the nervous system with a contraction. Muscle tissue can be classified into three types according to its function and to the structure of the cells composing it [1]:

- **Skeletal Muscle**
  The skeletal muscles are attached to the bones thanks to the tendons, therefore with their contraction they can modify the orientation of the bones, keeping the posture and allowing voluntary movements of the body. They also participate in thermal homeostasis, because with their contraction they generate heat as a by-product.
  Looking at a skeletal muscle cell under a microscope, it will appear with prominent striation, due to the alternation of the contractile proteins actine and myosin; it is also possible to observe the presence of many nuclei squeezed along the membranes, due to the fusion of the many cells composing each long muscle fiber.
  This type of muscle will be further described in section 1.1.1

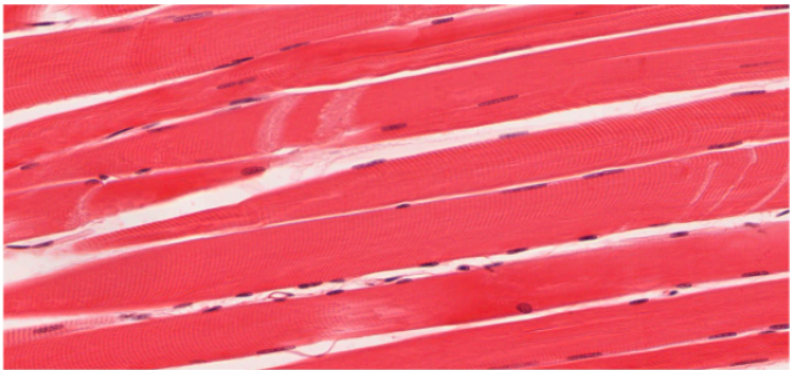

Figure 1.1: Skeletal muscle cells [1]

- **Cardiac Muscle**
  The cardiac muscle cells, also called cardiomyocytes, form the contractile walls of the heart. Their contraction is not linked to an external voluntary stimulus, but follows their own intrinsic rhythms. This is possible thanks to a specialized excitatory and conductive system peculiar to the heart: the rhythmical impulses are generated in the sinoatrial node and they are conducted through specific pathways to the atrioventricular node. There the impulses from the atria are delayed, before reaching the ventricles through the atrioventricular bundle, and being finally conducted to all parts of them thanks to the Purkinje fibers [15].
  Cardiomyocytes also will appear striated under a microscope, but unlike skeletal muscle cells they are single cells and their nuclei are centrally located.

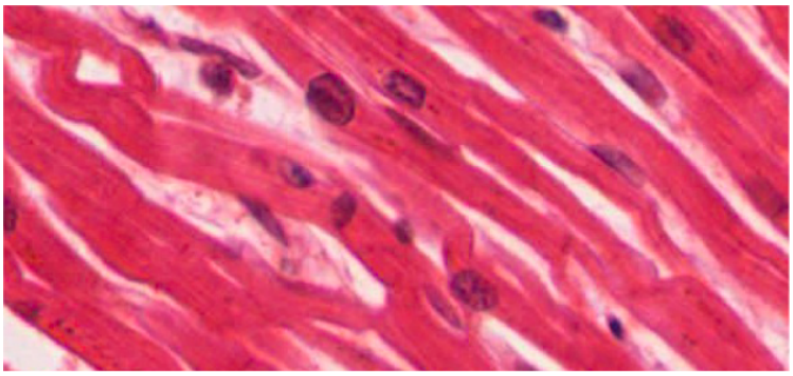

Figure 1.2: Cardiac muscle cells [1]

- **Smooth Muscle**
  The smooth muscles form the contractile component of the digestive, urinary and reproductive system, as well as the walls of the arteries, the airways and

generically of every hollow visceral organ in the body, except from the heart. Their contraction is responsible for involuntary movements in the internal organs, in fact it is controlled by the autonomous nervous system.
Smooth muscle cells have a single nucleus and, true to their names, they don not present visible striations.

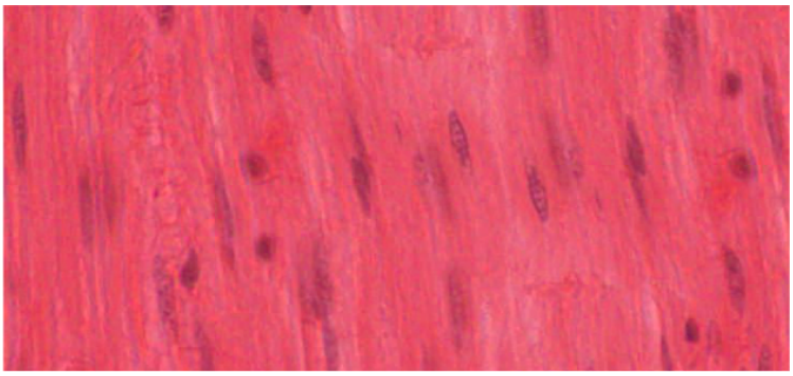

Figure 1.3: Smooth muscle cells [1]

1.1.1 The Skeletal Muscle

This thesis will often deal with *ElectroMyoGraphy* (EMG), in particular with the generation and the analysis of EMG signals. Most EMG signals represent the electrical activity of the skeletal muscles, therefore it is important to focus on the main physiological and anatomical aspects of such kind of muscles.
About 40 % of the body is made of skeletal muscles, and another 10% of smooth and cardiac muscles. If we do not consider water, that is the primary constituent of most tissues (in the case of the skeletal muscle it makes up the 75% of it), proteins are the main component of the muscles. In fact, 20% of the muscles is made by proteins, with the remaining 5% containing other substances like fat, carbohydrates, inorganic salts and minerals. 50 - 75 % of all body proteins are contained in the muscles [16].
As stated before, skeletal muscles are involved in numerous body functions. From a mechanical point of view, their main goal is to convert chemical energy into mechanical energy, that will be used to generate force and power. Another function is maintaining posture an moving the different parts of the body by modifying the orientation of the bones. From a metabolic point of view, skeletal muscles act as a deposit for fundamental substrates as carbohydrates and amminoacids, contribute to the basal metabolism, to the generation of heat for homeostasis and to the consumption of oxygen and nutrient during physical activity [16].

Anatomical classification of the Skeletal Muscles

The skeletal muscles can be classified in different ways according to the parameter that is analyzed. According to their shape, the muscles can be divided into *long muscles*, *flat muscles* and *short muscles*: long muscles can be found in the limbs and in some cases in the torso and head, where superficially flat muscles are more present; short muscles instead are mostly in the torso, in a deep position.
According to their position, we have superficial and deep muscles. Superficial muscles are located right under the skin, and they are attached with at least one of their extremities to the lower face of the dermis; facial muscles and muscles of the head and neck are the main superficial muscles. Deep muscles are located under the hypodermis (the lowermost layer of the integumentary system): most of them (the majority of the skeletal muscles) are attached directly or not to bones, cartilages or ligaments; other deep muscles can be attached to sensory organs, like the muscles of the eyes, or to mucous membranes of other systems, like the intrinsic tongue muscles. [17]
Skeletal muscles are composed of numerous fibers, grouped in fascicles and made up of successively smaller sub-units (this organization will be further described in the following paragraphs). The muscle fibers are parallel with regard to the other fibers composing the same fascicle, but the disposition of the fascicles within a muscle and in relation to the direction of the pull varies from one muscles to another, and allows to divide skeletal muscles in four categories [4]:

- **Parallel Muscles**: the fascicles are parallel to the longitudinal axis of the muscle, and when the fibers contract together the entire muscle shortens by the same amount. An example of parallel muscle is the biceps brachii.
- **Convergent Muscles**: the fibers are spread out over a broad area, but they all come together at a common attachment site. They are quite versatile, as they can change the direction of the pull by employing only one group of muscle cells at a time. An example of convergent muscle is the prominent pectoralis muscle of the chest.
- **Pennate Muscles**:the fibers are arranged like a feather, they sit at an angle and attach to a tendon long as the whole muscle. A pennate muscle contains more fibers than a parallel one of the same size, so its contraction produces more tension. An example of pennate muscle is the rectus femoris.
- **Circluar muscles**, also called *sphincters*: the fibers are concentrically arranged around an opening; the contraction of the fibers decreases the diameter of the opening. An example is the orbicularis oris of the mouth.

Skeletal muscles can also be classified according to the primary action that derives from their contraction [4]:

- An **agonist** is a muscle whose contraction is mostly responsible for producing a particular movement.
- An **antagonist** is a muscle whose action opposes that of the agonist.
- A **synergist** , that with its contraction assists the agonist in performing the action, stabilizing the origin or providing additional pull to the movement.
- Agonists and antagonist can contract simultaneously to stabilize a joint; in that case they are acting as **fixators**.

Gross Anatomy of the Skeletal Muscle

Various integrated tissue are involved in the composition of a skeletal muscle, including the skeletal muscle fibers, nerve fibers, blood vessels and connective tissue. Three layers of connective tissue enclose every skeletal muscle, providing it structure and compartmentalising the muscle fibers within it.

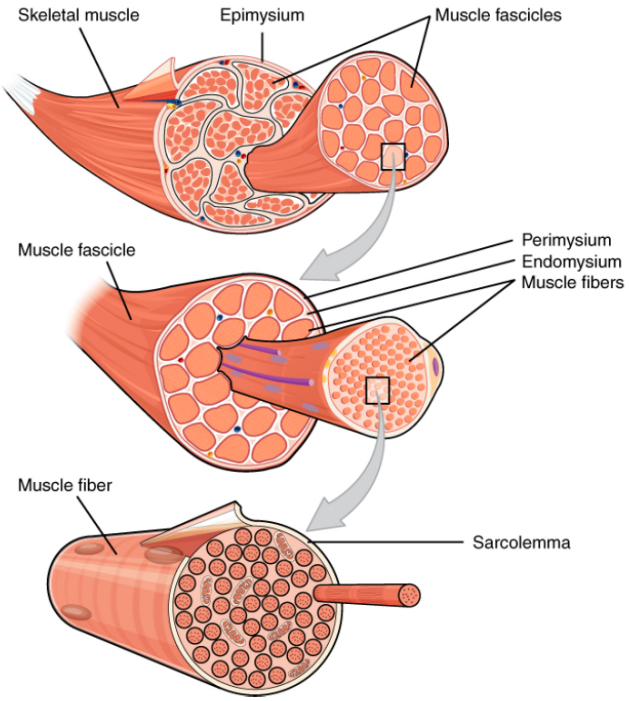

Figure 1.4: The three connective tissue layers in the skeletal muscles [2].

Each muscle is wrapped in the **epimysium**, a sheat of dense, irregular connective tissue that maintains the structural integrity of the muscle but still allows it to contract and move. The epimysium also separates the muscle from the surrounding tissues and organs, making so that its movement can be independent. Inside each skeletal muscle, a second membrane called **perimysium** divides the muscle fibers into individual bundles, called **fascicles**. This fascicular organization makes it possible for the nervous system to activate separate subsets of muscle fibers within a bundle, or of fascicles within a muscle: in this way the nervous system can trigger specific movements. Inside each fascicle, the **endomysium**, a thin connective tissue layer of reticular fibers and collagen, encloses each muscle fibers, and contains the nutrients to support the muscle fibers. Every muscle fiber is linked to the axon branch of a somatic motor neuron, which stimulates the contraction of the fiber. Skeletal muscles are also supplied by blood vessels for oxygen delivery, nourishment and waste removal [2].

Microanatomy of Skeletal Muscle Fibers: myofibrils and sarcomere organization

Muscle fibers range from 10 to 80 micrometers in diameter, they are usually long as the whole muscles, so they can reach a length of 30 cm in the longest muscles like the Sartorius of the leg. A single muscle fiber is enclosed by the **Sarcolemma**, a thin membrane with an outer coat that contains numerous thin collagene fibrils.

Every muscle fiber is composed of several hundreds to several thousands **myofibrils**. Each of them contains about 3000 **actine** filaments and 1500 **myosin** filaments: actin and myosin are two protein responsible for the muscle contraction. As we can see in figure 1.5, myosin is a thick filament, while actin is thin. Myosin and actin filaments partially intersect with one another, therefore myofibrils have alternate "light" and "dark" bands (figure 1.6). The light bands contain only actin filaments, while the dark ones contain myosin filaments but also the ends of the actin filaments, where they overlap the myosin. The bands are named according to their reaction at polarized light: the light bands are called *I bands* because they are *isotropic* to polarized light, while the dark bands are called *A bands* because they are *anisotropic* to it. Small projections called *cross-bridges* expand from the side of the myosin filament: their interaction with actin filaments causes contraction. The extremities of the actin filaments are attached to a *Z disk*, which is composed of other filamentous proteins and passes crosswise across the myofibril and from one myofibril to the other, connecting them all the way across the muscle. The portion of myofibril between two consecutive Z disks is called **sarcomere**. The sarcomere shortens when the muscle is contracted and it can reach a length of about 2 μm :

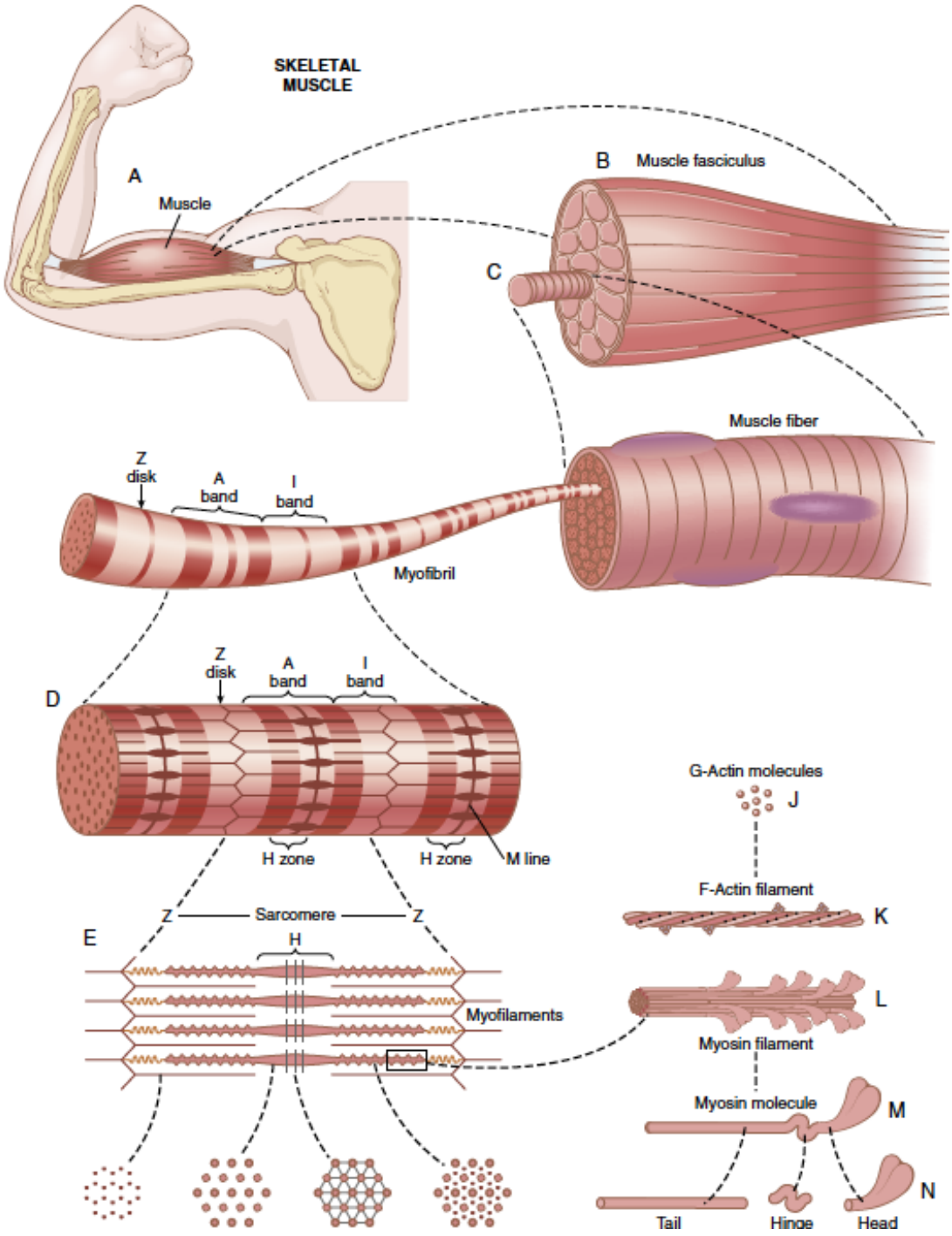

Figure 1.5: Organization of skeletal muscle, from the gross to the molecular level. [3]

in this situation actin and myosin filament are completely overlapped [3].

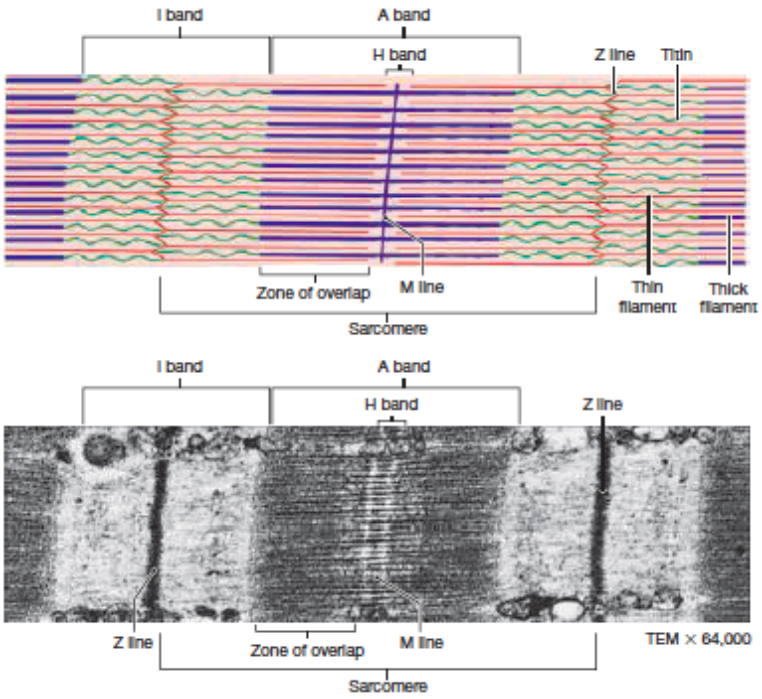

Figure 1.6: A transmission electron microscope image of a sarcomere in the gastrocnemius of the calf, with a diagram illustrating its components [4].

The interaction between actin and myosin is regulated by a filamentous and springy molecule called **titin**, that holds them in place so that the contraction can happen. One extremity of the titin molecule is attached to the Z disk, and thanks to its

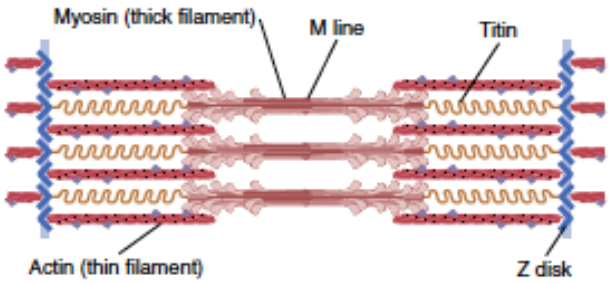

Figure 1.7: Organization of proteins in a sarcomere [3]

elasticity changes length as the sarcomere contracts and relaxes; the other end is linked to the tick filament of myosin (figure 1.7). The space between the many myofibrils in each muscle fiber is filled with the intracellular fluidi *sarcoplasm*: it contains multiple protein enzimes and large quantities of phosphate, magnesium

and potassium. It also contains a very high number of *mitochondria*, fundamental for the supply of the large amount of energy needed for the contraction, that they deliver through the production of adenosine triphosphate (ATP) [3].

General mechanism of muscle contraction

All cells are characterized by an electrical gradient across their membranes, also called membrane potential: the difference of potential between the inside and the outside of a cell is usually around -60 to -90 mV. Muscle cells and neurons take advantage of this potential to generate electrical signals, by controlling the flow of ions across their membranes. The movement of these charged particles is regulated by opening and closing of specialized proteins in the membrane, the ion channels. The capability of both skeletal muscle cells and neurons to generate action potentials makes them electrically excitable. An action potential is a kind of electrical signal that is able to be transmitted along a cell membrane in a wave-like pattern. Thanks to them it's possible to transmit a signal in a quick and faithful way also over long distances. The contraction of a skeletal muscle fiber must be triggered by an action potential, whose transmission along the sarcolemma generates a series of events at the molecular level, that will be further described, that lead to the shortening of the muscle fiber. In the skeletal muscles, the action potential originating the sequence of events leading to the contraction of the muscle is generated in the somatic motor division of the nervous system, specifically in motor neurons that are originated in the spinal cord (with the exception of a smaller number located in the brainstem that control the activation of the muscles of the face, head and neck). The transmission of the action potential across such long distances happens thanks to the long axons of these neurons [2].

The action potential triggering the contraction travels along the motor nerve until it reaches its endings, located on the muscle fiber. In correspondence of every of these endings, the nerve secretes a small quantity of the neurotransmitter *acetylcholine*, that opens acetylcholine-gated cation channels located across the muscle fiber membrane. Through these open gates, large quantities of sodium ions move to the interior of the membrane. This leads to a local depolarization, that causes to the opening of voltage-gated sodium channels, that will be responsible for the initiation of an action potential. The action potential depolarized the muscle membrane, and its electricity reaches the center of the muscle fiber. Reacting to this flow of action potential, the sarcoplasmatic reticulum releases a large number of calcium ions that were previously stored in it. The calcium ions generate the contractile process of the actin and myosin filaments, causing them to slide one along the other. After a fraction of second, a Ca^{2+} membrane pump brings back the

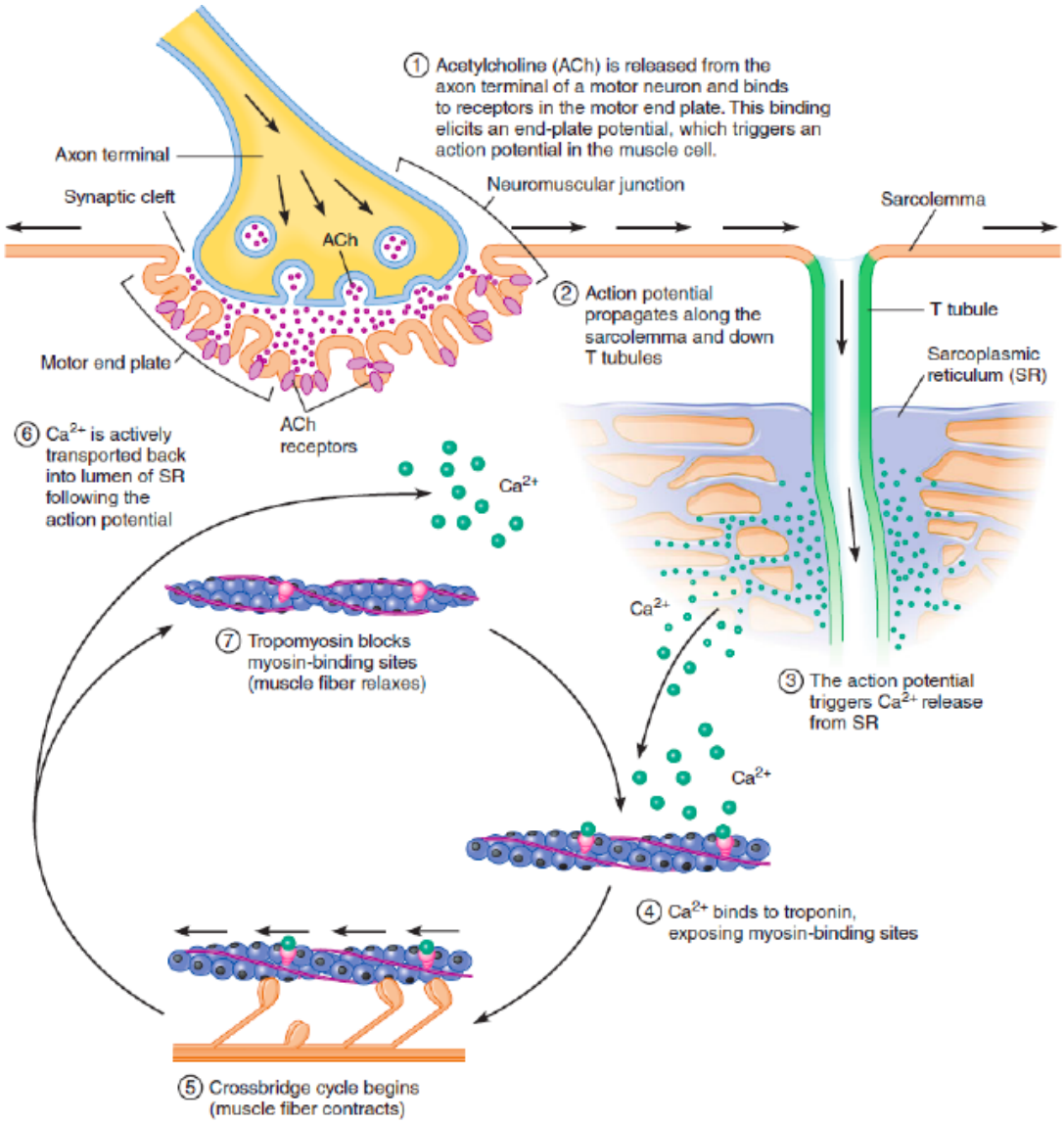

Figure 1.8: Muscle contraction mechanism: from the motor neurons to the molecular mechanism [5]

calcium ions in the sarcoplasmatic reticulum, where they will remain stored until the next action potential. Because of the removal of the calcium ions from the myofibrils the muscle contraction ends.[3]

Types of muscle fibers

Muscles can be composed of a mixture of three types of muscles fibers: the distribution of these fibers will determine the action of the muscle. The main differences

between the three types are in how they get their ATP supply.

- **Fast fibers**, or *white fibers*, are large in diameter, have densely packed myofibrils, their concentration of mitochondria is relatively low, while glycogen is highly present. They are named "fast fibers" because they react quickly to stimulation with a contraction. The tension delivered by a muscle fiber is directly proportional to the number of myofibrils, so this kind of muscles deliver powerful contractions. However, their few mithocondria are not able to provide the quantity of ATP needed, and *anaerobic metabolism* (glycolysis) is necessary to guarantee the contractions. Glycolysis, without needing oxygen, converts the glycogen supplies to lactic acid. The build up of lactic acid, that interferes with the contraction mechanism because of its pH, makes so that fast fibers reach fatigue rapidly.

- **Slow fibers**, or *red fibers*, have a smaller diameter, their contraction is much slower, but longer. They contain a larger number of mithocondria, so they continue to produce ATP during the contraction for a longer time, making so that red fibers reach fatigue slowly and can therefore continue to contract for a longer time. Mithocondria absorb oxygen, generating ATP with an *aerobic metabolism*. The large amount of oxygen present comes from two main sources: the oxygen bounded to the myoglobin proteins, that have a high concentration in the red muscles; the oxygen delivered from the red blood cells, greater then for the white fibers because muscles made of red fibers contain a larger network of capillaries, and there is grater blood flow to the muscle.

- **Intermediate fibers**, that have properties between those of fast and slow fibers. This makes them adaptable to different situations, but still able to specialize in response to particular requested efforts. [4]

The majority of muscles contain a combination of all three fibers, but a bundle of fibers within the same motor unit must be of the same type. For each muscle, the percentage of fast versus slow fibers is genetically determined, with significant differences among individuals.

Mechanics of contraction

The length and the strength generated by a muscle contraction can be very different across different contractions. The mechanism involved in the control of the amount of force generated by a single contraction is called *summation*, and it can occur in two ways [3]:

- **Multiple fiber summation**. Each motoneuron starts from the spinal cord and reaches multiple muscle fibers: all the fibers innervated by a single neuron make up a *motor unit*, together with the neuron itself and the neuromuscular junctions involved. The number of fibers in a motor unit depends on the dimension and function of the muscle. The recruitment of the motor units to respond to a stimulus from the central nervous system follows the *size principle*: at first the smaller motor neuron are stimulated, then as the strength of the signal received increases, the motor neurons involved become larger and larger. This phenomenon allows the gradation of muscle force to start in small steps that become progressively larger when larger amount of force are needed.

- **Frequency summation and tetanization** When the frequency of stimulation is low, individual twitch contractions (figure 1.9.1) are separated in time by a latent period. Increasing the frequency, at some point it will happen that each new contraction starts before the previous one is over: the second contraction is partially added to the first and the total strength becomes higher as the frequency increases. At a certain critical level of the frequency, the successive contractions become so close that they fuse together, in a contraction that appears smooth and continuous (as shown in figure 1.9.4): this phenomenon is called *tetanization*. The maximum strength of the contraction has been reached, and it cannot increase even if the frequency becomes higher, therefore tetany corresponds to the maximum force that the muscle can generate.

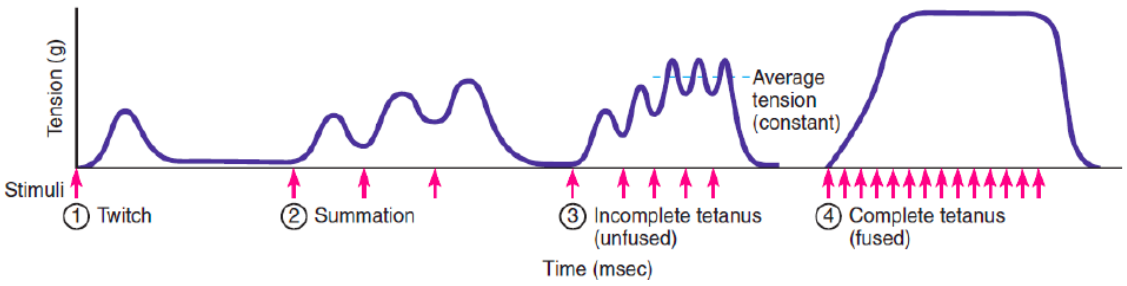

Figure 1.9: Muscle stimulation: frequency summation and tetanization [5]

1.2 Surface Electromyography (sEMG)

ElectroMyoGraphy is a diagnostic and investigation technique where the electrical signal derived from the contraction of a skeletal muscle is recorded. Every EMG

signal is generated by the propagation of an action potential (AP) from the neuromuscular junction to the tendon of the muscle. The smallest functional unit of a muscle that can be subject of a voluntary contraction is the *Motor Unit* (MU), that anatomically is composed by all the muscle fibers innervated by the same motoneuron. The signal obtained summing all the APs that arrive to a motoneuron is called Motor Unit Action Potential (MUAP). It has been proved that the EMG signal derives from the combination of all the electrical contributes of each motor unit that has been recruited for the contraction [18].
There are two different types of EMG:

- **Intramuscolar ElectroMyoGraphy (iEMG)**
  This technique is the classic and oldest way in which EMG signals were detected. The instrumentation involved are needle electrodes, that passing through the skin are directly placed into the muscle to be analyzed. Since the distance between the electrodes and the source of the signal is very short, this technique is characterized by a high volume selectivity, and therefore is particularly suited for the recording of a single MUAP. From the signal extracted it

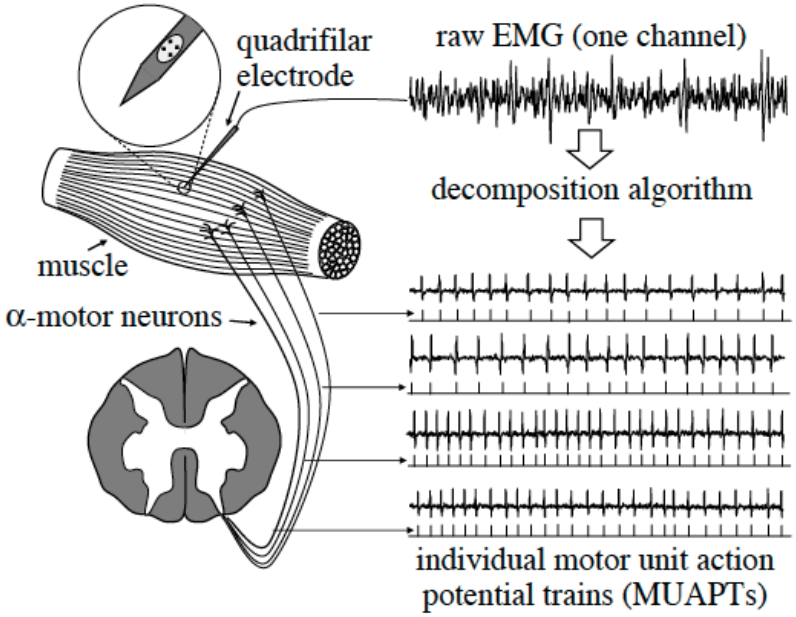

Figure 1.10: Intramuscolar ElectroMyoGraphy (iEMG) [6]

is possible to separate the contributions of the single units (figure 1.10), so it is possible to identify both the morphology and the temporal activation of the signal. Another advantage of this technique, due to the fact that the electrode is in direct contact with the muscle, is the absence of any filtration or artefact

caused by the surrounding tissue. However, iEMG presents several disadvantages, such as the need to sterilize needles at every use, the high invasiveness of the electrodes, and the fact that the techinque cannot be applied during dynamic motor activity.

- **Surface ElectroMyoGraphy (sEMG)**
  The electrodes for the recording of the EMG are placed directly on the surface of the skin, above the interested muscle: this technique is less invasive and suitable for superficial muscles. The number of electrodes used can vary from the basic two needed to a complex array of electrodes. The positioning of the electrode is crucial for the quality of the recorded signals: the skin must be properly prepared, the stability of the interface with the skin must be as high as possible and the electrode must be positioned in exact correspondence with the muscle of interest. The recorded signal is an interference signal given by

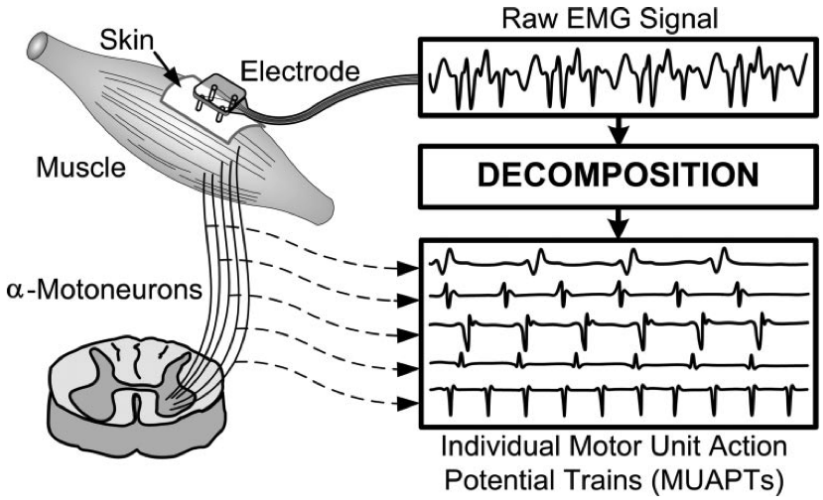

Figure 1.11: Surface ElectroMyoGraphy (sEMG) [7]

the algebraic sum of all MUAPs of the involved motor units. It is possible to trace back the action potential of the single motor unit through decomposition techniques [7]: this allows to understand the recruiting method of the analyzed muscle and so its specific functioning. The extraction of the single MUAPs is less accurate than the one obtained from iEMG signals, but sEMG performs better in recording the overall activity of a muscle or muscle group. The main advantage of the sEMG over the iEMG is the possibility of performing dynamic and long-lasting tests without distressing the subject with needle injection. For these reasons, sEMG is widely used in clinical applications and rehabilitation.

1.2.1 Acquisition of sEMG signals

The acquisition set-ups for the sEMG signals differ one from the other for both the material and the dimensions of the electrodes, their configuration and their positioning.
The most common surface electrodes are made of silver (Ag), silver cloride(AgCl), silver/silver cloride (Ag/AgCl) or gold (Au). The most used are the Ag/AgCl: since they are almost non-polarizable they make so that the surface potential is less sensitive to sliding movements between the skin and the electrode surface. The stability of the skin-electrode interface can be enhanced interposing a conductive gel layer. The size of the electrode can vary from millimeters to a few centimeters in diameter or length (depending on the shape) depending on the field of application. The choice of the dimension of the electrodes must take into account the depth and dimension of the muscle, its architecture and the desired spatial resolution. [8]
Two recording modes are possible: *monopolar* and *bipolar*. In the monopolar mode,

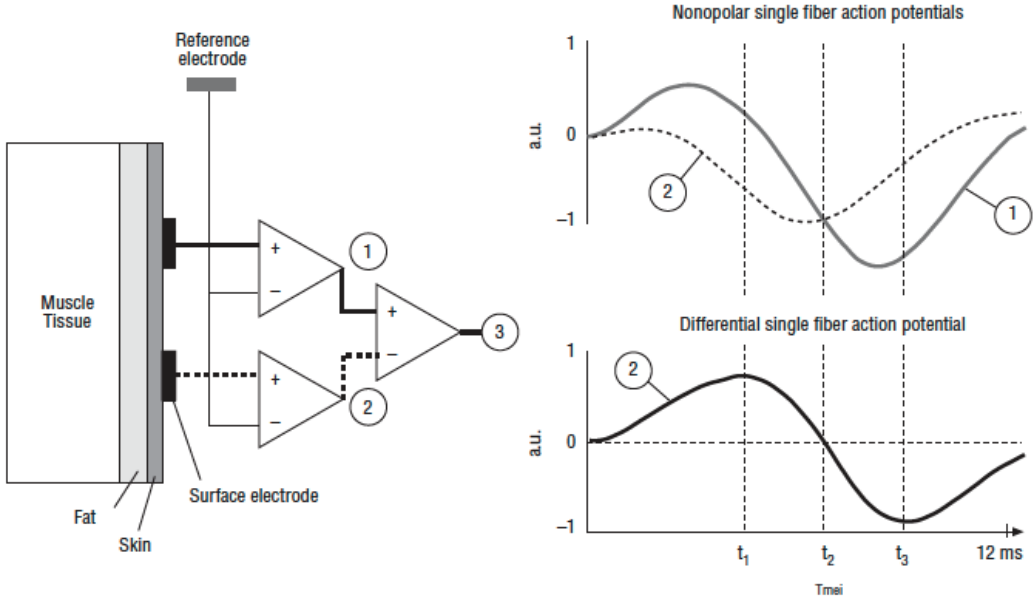

Figure 1.12: Electrodes configurations [8] On the left:mono-polar mode (block 1) and bipolar mode (block 1 + 2 + 3). On the right: mono-polar signals 1 and 2: their subtraction would give a bipolar signal

an active electrode is placed on the skin surface above the muscle and a reference electrode is put above bony regions of the skin. A large volume of sampling is guaranteed in this configuration, meaning that also more disturbances are collected and spatial filtering is absent. In the bipolar mode, a second active electrode is used above the same muscle, and the signal is given by the subtraction of the two

monopolar signals. This reduces the volume of sampling, so this mode is less subject to disturbances, but is less selective and also some components of the signal are lost. [8]

The sEMG signal is a stochastic signal that can be reasonably represented by a Gaussian distribution function. Its amplitude can vary in a range from 0 to 1.5 mV (RMS) or from 0 to 10 mV (peak-to-peak). The frequency content of the signal is in the range from 0 to 500 Hz, but the spectral components with a higher power are in the 50-150 Hz range [9]. An example of a frequency spectrum of an sEMG signal is represented in figure 1.13.

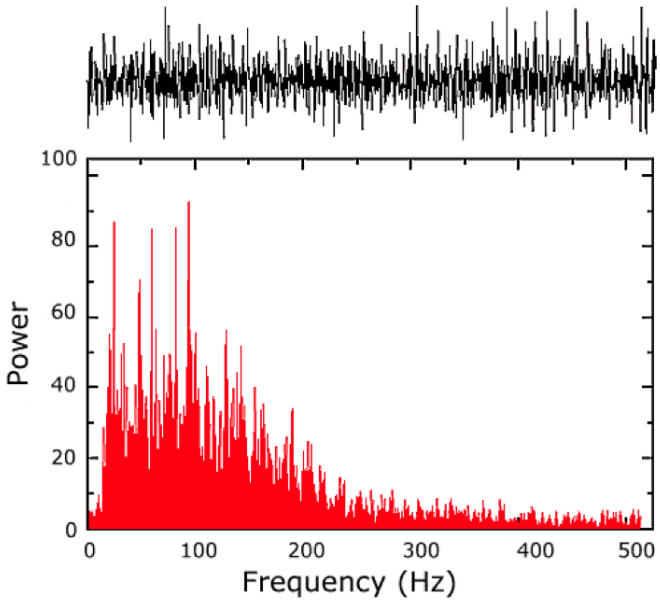

Figure 1.13: Frequency spectrum of an sEMG signal [9]

The block diagram of a sEMG acquisition chain is shown in figure 1.14
The first block, the *amplification*, is a differential amplifier that multiplies by a fixed gain the difference between the two collected signals. This step has the aim of amplifying the sEMG signal in a way that its amplitude can match the range of the A/D converter, so that is possible to digitize in a sensible way even small fluctuations of the sEMG.
The second block, the *filtering*, is necessary to remove the *aliasing* disturb, due to the presence of higher frequency components above the upper limit of the frequency band of the sEMG. The filter used is usually a low-pass filter with a cut-off frequency of 400 Hz.
The digitization of the signal is performed by the *A/D Converter*. The crucial

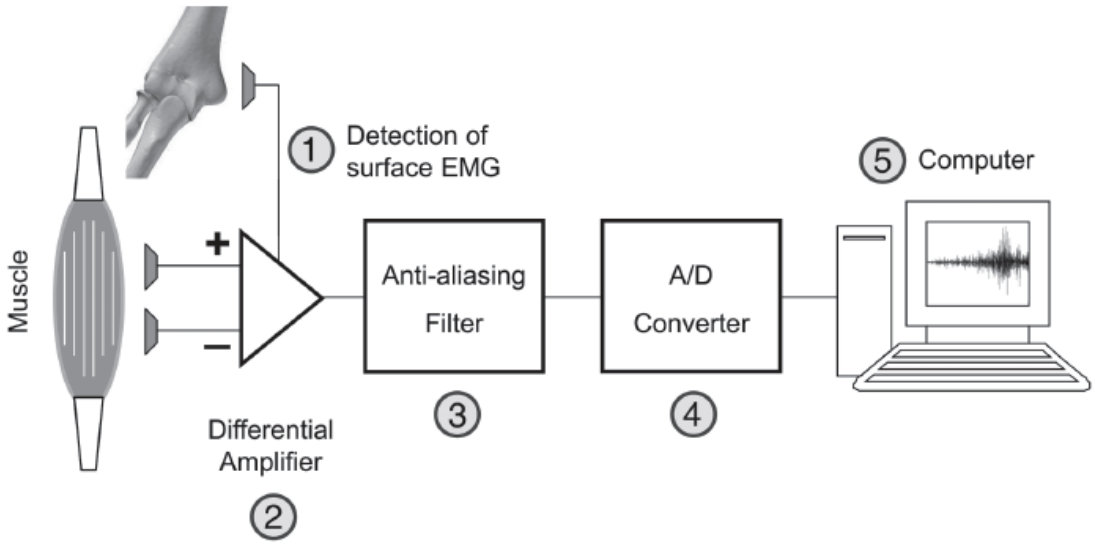

Figure 1.14: sEMG signal acquisition chain [8]

parameter of the converter is its resolution, defined by the ratio between its dynamic range and the number of levels; the resolution indicates the smaller variation that the system is able to record. The A/D converter samples analogical data and converts it to digital data, with a specific sampling frequency that must satisfy the Nyquist theorem. Additional filtering operations that could be needed to remove certain frequency components can be performed after the recording with digital filters [8].

1.2.2 Noise sources in sEMG signals

The main sources of noise afflicting the recording of sEMG signals and decreasing the fidelity of the signal are [9] [19]:

- **Inherent Noise due to the electronic components**: refers to the electrical noise generated by the electronic instrument involved in the detection and recording of the signal. The frequency of this noise ranges from 0 Hz to several thousands Hz. This noise cannot be eliminated, but it can be reduced designing the circuit in the most efficient possible way and using electronic components with a quality as high as possible.
- **Motion Artefacts**: they can be due to the movement of the cables connecting the electrodes to the circuit or to the sliding movement of the electrode on the skin, caused to the change in muscle length during the contraction. The first problem can be reduced designing a suitable circuit, the second by interposing

a gel layer in the skin-electrode interface. The frequency of this noise is usually low, below 15 Hz.

- **Ambient noise**: caused by the interference between the acquisition devise and the elements in the external environment that produce electromagnetic radiations (antennas, power supply, light bulbs, etc). These disturbs have an amplitude about three times larger than the sEMG signal, so it is necessary to reduce them in the post processing with filtering. The most peculiar ambient noise is the Power-Line Interference (PLI) which has a frequency of 60 Hz in the USA and of 50 HZ in the EU.

- **Inherent instability of the signal**: due to the naturally statistical behaviour of the amplitude of the EMG signal. The frequency components between 0 and 20 Hz are unstable because they are affected by the firing rate of the motor units, which is almost random. It is advisable to remove these components from the signal.

- **Cross talk**. More than one muscle is active during the same movement: cross talk happens when, during the recording of an sEMG signal, the electrode detects also the activation of a neighbour muscle. This causes a misinterpretation of the signal. At the moment there are no available methods to eliminate cross talk after the signal recording, so it must be reduced while collecting the signal, with precautions on the inter-electrode distance and on their size.

- **ECG artifacts**: the electrical activity is a strong source of noise, mainly for sEMG signals taken from trunk level muscles. There is no way to eliminate it completely after the recording, but it can be reduced using a high CMMR acquisition channel.

Chapter 2

Muscle Synergies

Every voluntary movement performed as a reaction of a stimulus by the Central Nervous System (CNS) involves a large number of muscles, each of them containing thousands of motor units, whose contraction must be neatly modulated and coordinated in order to achieve the planned action. The inverse dynamic problem that must be solved by the CNS even only for the realization of a simple motion is related to a high number of Degrees of Freedom (DoF), needed to control all the kinematic and kinetic parameters. In fact, in the musculoskeletal system there are more muscles then corresponding joints, and the same movement can be achieved by a wide range of combinations of muscle patterns.

Understanding how the CNS deals with the redundancy of the musculoskeletal system and reduces the complexity level behind every movement has been a pivotal goal in neuroscience, and it has opened a novel clinical scenario in the treatment of motor impairments caused by a malfunctioning of the CNS [10]. Starting with *Bernstein* in 1967 [20], a lot of researchers have tried to understand how the CNS is able to reduce the computational burden linked with the generation of a movement, searching for physiological evidence of simplifying strategies. The concept of *Muscle Synergies* has been introduced: they can be defined as a block of muscles activated, to different levels, at the same time to reach a generic movement, thus reducing the computational cost of the task performed by the CNS, since it has to control a group of muscles instead of a single one [21].

In the last two decades, many experimental studies have supported the validity of this modular approach, both in humans and in animals, and also its possible alterations due to neural injuries, causing pathological behaviors and altered movements. Therefore, the analysis of muscle synergies can be regarded as a useful diagnostic tool in the assessment and rehabilitation of neuromotor diseases [10].

2.1 Synergies and Motor Control

The synergistic hypothesis represents the synergies as direction of the motor control employed by the CNS, as modules combined together in order to rise complex movements. The synergies reduce the volume of the space motor command that the CNS needs to investigate, reducing the complexity of the problem. Intrinsic in the definition of synergies is therefore the fact that the number of muscle synergies must be lower than the number of muscles involved, otherwise their meaning would be lost [10].
Muscle synergies give information about which muscles are grouped, because muscles that appear to be co-activated at the same time are grouped under the same synergy, but also on "how" these muscles work together. In fact, each synergy expresses also the contribution that each muscles brings to the synergy it belongs to, and this aspect is described by the "weights" aspect of a synergy [10]. This is represented by the "weighted connections" in figure 2.1.

A valid theory for motor control is the hierarchic control theory, a complex circuitry extending from motor cortex to spinal neurons. A voluntary movement is realized as a consequence of the correct time activation of spinal inter neuronal muscle synergies by the motor cortex, which handles the modules with specific time activation patterns in order to achieve a precise motor task [10] (figure 2.1). Muscle synergies can be extracted from EMG signals to observe in a tangible way the validity of the theory. Each synergy can be modeled as a synchronous, time-invariant activation profile across the muscles, where each muscle could potentially be part of more than one synergy. Each synergy is activated by a non-negative, time-varying action coefficient: the final EMG signal can be reconstructed by linearly combining the activation signals weighting them by the corresponding time-varying coefficients. [22] A scheme of this model is displayed in figure 2.1.
This model can be represented analytically as:

$$\mathbf{M}(t) \simeq \sum_{i=0}^{N} \mathbf{c}(i) \times \mathbf{W}(i) \tag{2.1}$$

where *M(t)* is the muscular activity, *c(i)* the time activation pattern of the specific muscle synergy, *W(i)* represents the $i^{(}th)$ synergy vector and N is the total number of muscle synergies.

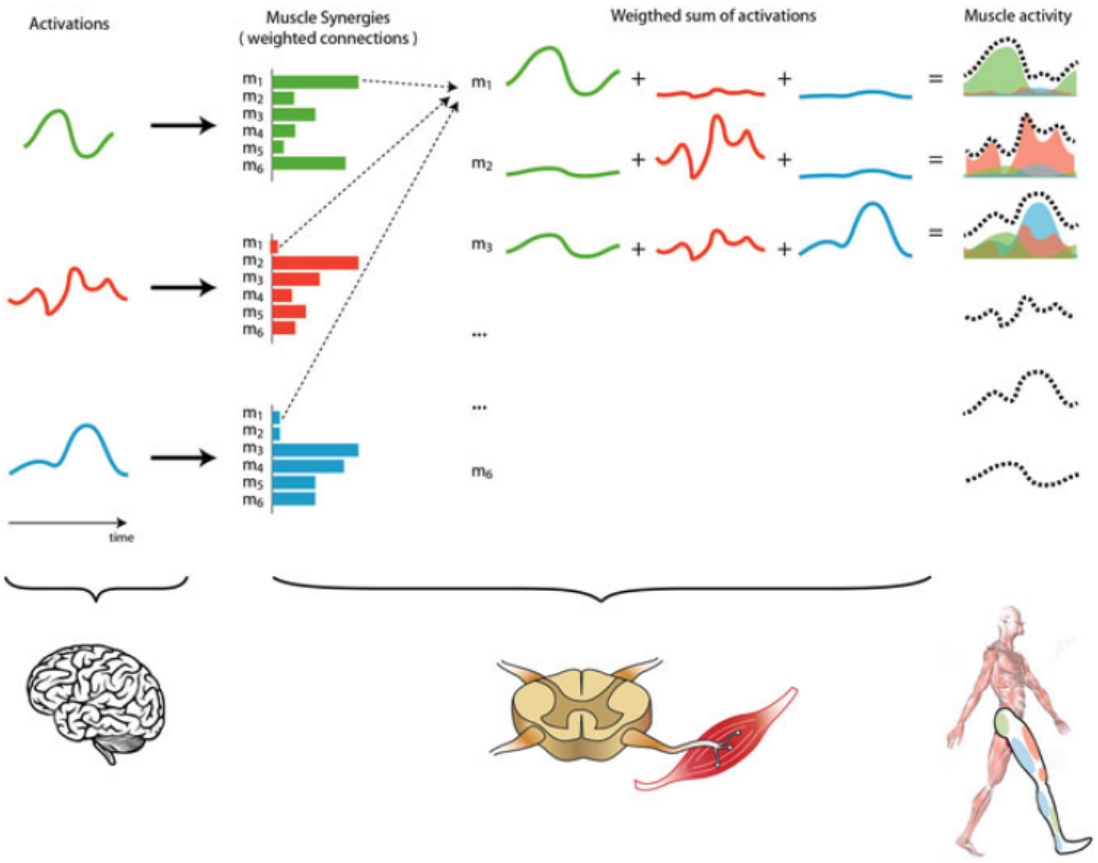

Figure 2.1: Muscle synergies hypothesis: muscle activity result from a linear combination of time activation signals and muscle synergies weights [10]

2.2 State of the art

The first studies to understand the neural origin of the synergies, considered as motor modules, involved studies on the spinal cord in several vertebral species, applying different stimulation techniques [21]. It was possible to observe experimentally the modular organization of the spinal cord circuitry in the frog [23] [24], in the cat [25] and in the rat [26]. A growing number of studies have given evidences for the synergistic hypothesis also in humans, showing that it is possible to reconstruct muscle activation patterns with a number of synergies smaller in a variety of behaviour and tasks [10]. Muscle synergies were observed in the activity of the muscles of the lower back and of the leg to guarantee human postural control [27] . In [28] five muscle activity patterns were found in human physiological gait, observing their invariance even in different conditions of walking speed or body weight. Differences between these patterns in walking and running was

analyzed in a successive study by the same group [29], while in [30] the activity of cycling was considered, observing wether muscle synergies are constrained by changes in the mechanics of pedaling. Several studies were performed also on the upper limbs: the synergies controlling both movement and posture of the muscles involved in natural reaching movements at different speeds were studied in [31]; synergies involved in postural control of the movements of the hand and its fingers were observed in [32]; force control in isometric contractions was analyzed in [33].

The high potential of the use of Muscle Synergies as an assessment tool for neurological pathologies was soon explored. In disorders of the CNS caused by strokes or spinal cord injuries (SCI), several motor deficits are present because of inappropriate muscle activity and coordination. Muscle synergies may be used to evaluate the modification in the physiological muscle activity and to provide a better understanding of these deficits. [10].
Ivanenko et al [34] analyzed lower limb muscle synergies obtained from 11 SCI patients, with different levels of sensory and motor impairments. EMG signals were collected during treadmill walking aimed at the reproduction of a foot kinematics as similar as possible to the physiological ones, at different speeds and different levels of body weights support. Comparing the obtained synergies with the ones of healthy subjects, it was found that the structure of the muscle synergies was altered, but the temporal activations were preserved; in particular, in less impaired subjects the similarity with the synergies of the healthy subjects was higher than in the most affected patients. In another study [35], it was suggested that SCI patients may learn new motor patterns with training rather than re-activate physiological motor patterns, thanks to a reorganization of the connections of the interneuronal networks. These compensatory solutions lead to new muscle synergies, but in general the temporal patterns of the activation coefficients are preserved.
Muscle synergies in post-stroke subject have also been investigated. Gizzi et al ([36]) analyzed the locomotion of 10 patients recently affected by strokes (at most 20 weeks before), collecting EMG signals from 32 muscles of the trunk, upper and lower limb during walking overground at comfortable speed. In the muscle synergies extracted it was observed that the temporal activations were mostly preserved, but the synergies extracted from the muscles of the affected side, even if similar across the different patients, were different from the ones of the healthy patients and of the muscles of the side unaffected by the stroke. The authors speculated that these changes may be the result of compensatory strategies carried out by the trunk and upper limbs musculature to preserve a locomotion as functional as possible.

Cheung et al [11] investigated the changes in the motor control behaviours inducted by cortical damage evaluating upper limb muscle synergies in 31 stroke patients with a wide range of unilateral motor impairment, recording the activity in both arms while executing reaching movements. They found out that, for less impaired subjects, the muscle synergies were similar for the affected and unaffected arms, but the muscle activation patterns were different. The synergies extracted

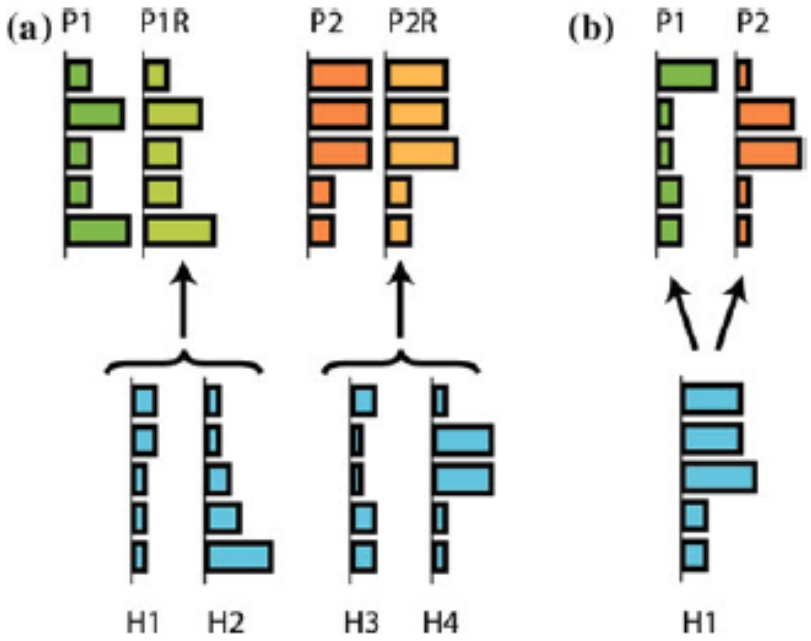

Figure 2.2: Merging and fractionation of muscle synergies. a) A Paretic side synergy may be explained as the merging of healthy synergies. For example, healthy synergies H3 and H4 can form P2R (paretic synergy reconstructed) by merging. b) Paretic synergies P1 and P2 can be derived from a fractionation of healthy synergy H1. [10] adapted from [11]

from the affected arms of severly impaired subjects showed three distinct behaviour: the preservation, the merging or the fractionation with respect to the synergies of the unaffected (healthy) arm. In the merging of muscle synergies, two groups of muscles normally independent become grouped. (figure 2.2a) The fractionation of muscle synergies happens when a group of muscles belonging to the same synergy is divided in two groups, with different modulation signals. (figure 2.2b)

2.3 Muscle Synergies Extraction

Muscle synergies are generally identified using several algorithms belonging to the class of *Matrix Factorization Algorithms*. From a mathematical point of view, the "matrix factorization" consists in the decomposition of a matrix into two matrices with lower dimensions whose product gives back the original matrix: it is basically a data projection from a n-dimensional space to a lower k-dimensional space. Considering n as the number of detection channels and k as the number of basis vectors, this approach can be applied to extract synergies: in fact, with this formulation it is possible to represent a complex motor task through a reduced number of muscle synergies. Several matrix factorization algorithms have been used to extract muscle synergies, such as the Principal Component Analysis (PCA), the Factor Analysis (FA), the Non-Negative Matrix Factorization (NNMF), the Independent Component Analysis (ICA) and the Probabilistic Independent Component Analysis (pICA). In a study by Tresch et al [37] the performances of those algorithm applied both on simulated and experimental data sets were compared, focusing on the ability of identifying sets of synergies from data sets with different features. It was observed that the performances of the five algorithms were similar and that they were all able to identify the correct synergies and activation coefficients in simulated data, as well as being consistent in the physiological data sets. This suggests that the muscle synergies found do not depend from the algorithm that was used, but they reflect the motor control patterns correctly.
A general model of any matrix factorization algorithm can be expressed as:

$$\vec{x} \simeq \sum_{i=1}^{K} c_i \overrightarrow{w_i} + \vec{\varepsilon} \tag{2.2}$$

where $\vec{x}$ is a matrix of M-dimensional data vector, $\overrightarrow{w_i}$ is the i^{th} out of K basis vectors, c_i is the scalar activation coefficient for the corresponding basis vector and $\vec{\varepsilon}$ models the noise contribute. Applying this model to the physiological context, $\vec{x}$ corresponds to the M muscles sEMG recorded activities and $\overrightarrow{w_i}$ are the muscle synergies activated by the temporal coefficients c_i. In this thesis, the algorithm that was used and analyzed is the Non-Negative Matrix Factorization (NNMF).

2.3.1 The Non-Negative Matrix Factorization algorithm

The Non-Negative Matrix Factorization is the most common algorithm used for the extraction of muscle synergies. [37] It is an algorithm that decomposes a matrix

into two non-negative matrices: one containing column vectors that are basis eigenvectors in the data space, one containing row vectors [38]. Due to the non-negative

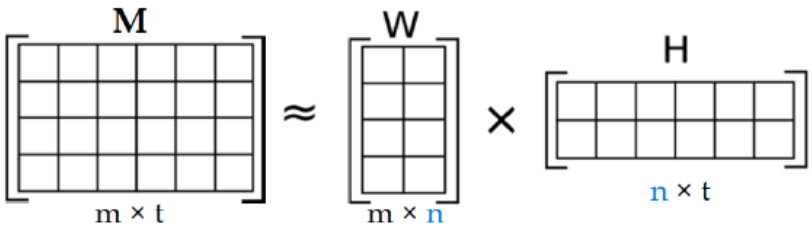

Figure 2.3: Factorization of Matrix M into two smaller matrices W and H [12]

constraint, the results of the NNMF algorithm are always positive and therefore easily suitable for practical applications.

A brief overview of the mathematical aspects of the algorithm is provided [39]. Given a data matrix V = [v_1,...v_j,... v_m] of dimensions n x m (where v_i are non-negative column vectors), the NNMF algorithm models the data as a linear combination of k basis column vectors of size n (k $\leq$ n) such that:

$$v_j = \sum_{i=1}^{n} h_{ij} w_i + \varepsilon_i \tag{2.3}$$

where w_i is the basis vector, h_{ij} the non-negative coefficient for the i-th basis vector corresponding to the data point j, and ε is a parameter that keeps into account the noise. Considering a matrix W = [w_1,...w_i,... w_k], the NNMF can be explained as the problem of finding the factorization of V in W and H [38].

$$V \approx WH \tag{2.4}$$

with H = [h_1,...h_j,... h_m] k x m matrix.
If ε is a Gaussian noise of constant variance [40], to determine the matrices W and H the follow multiplicative update rules are used [41] [42]:

$$H_{ij}^{S+1} = H_{ij}^{S} \frac{[(W^S)^T V]_{ij}}{[(W^S)^T W^S H^S]_{ij}} \tag{2.5}$$

$$W_{ai}^{S+1} = W_{ai}^{S} \frac{[V(H^{S+1})^T]_{ai}}{[W^S H^{S+1}(H^{S+1})^T]_{ai}}, a = 1, ...n, \tag{2.6}$$

where the superscript T denotes the transpose of the matrix, and the superscript S the number of current iteration of the updating. These are the traditional update rules for the NNMF algorithm.
To implement the algorithm, the number of basis vector k, that are the column vectors of the matrix W, needs to be known a priori. When applying the algorithm to extract muscle synergies, a criterion needs to be established to select the correct number of synergies. The trend of some parameters, like the Variance Accounted For (VAF) and R^2, the reconstruction error between the original EMG matrix V and the reconstructed EMG matrix WH (see chapter 3.1 for the mathematical definition of these parameters), can be used to define some criteria. Two common approaches are finding the smallest number of weight vectors such that R^2 is greater than a predefined threshold [11], or finding the model order for which R^2 reaches a plateau, so where a clear decrease of slope is observed [43]. A big limitation of both approaches is that these methods resulted to be very robust for simulated data sets [37], but not for real data sets.

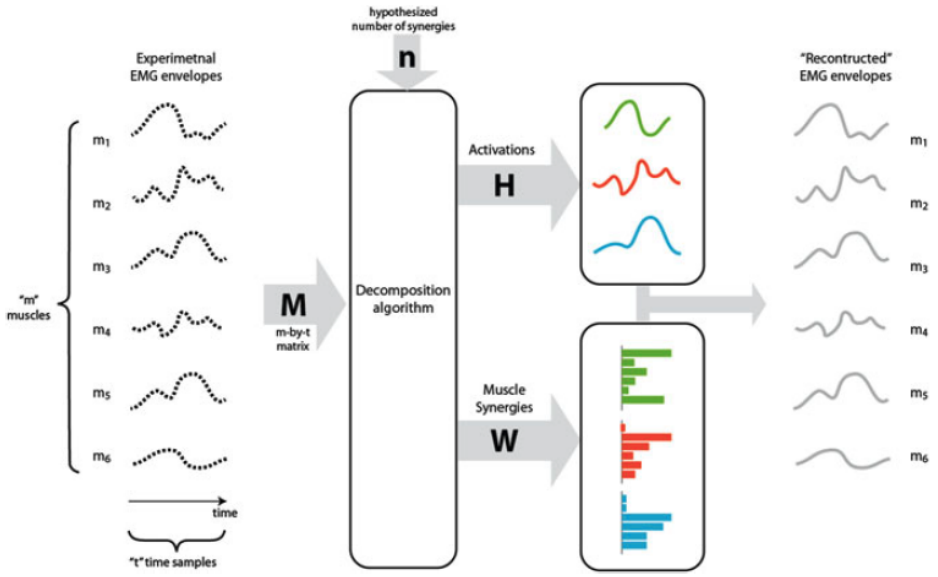

Figure 2.4: Example of factorization of matrix M into smaller matrices W and H, whose product gives back the original M matrix [10]

To concretely apply NNMF to real sEMG signals, it is necessary to obtain

their envelopes (see chapter 3.1) adapting them in a matrix **M** with m rows and t columns, with each row corresponding to the activity of the muscle during t time samples. The m-by-t matrix **M** is factorized into non-negative matrices **W** (m-by-n) and **H** (n-by-t), where n is the number of muscle synergies. The rows of matrix **W** represent the muscle synergies vectors that express the contribute activity of each muscle. Matrix **H** reports the temporal patterns of activation of every specific synergy. The process can be summarized in figure 2.4.

Chapter 3

Material and methods

3.1 Muscle Synergies Analysis

The procedure for the extraction of muscle synergies from EMG signals is outlined in figure 3.1. The first step is the recording of the muscle activity as EMG signals: the signals must then be processed so that they can be given as input to an algorithm, which will be responsible for the extraction of the synergies and their activations.

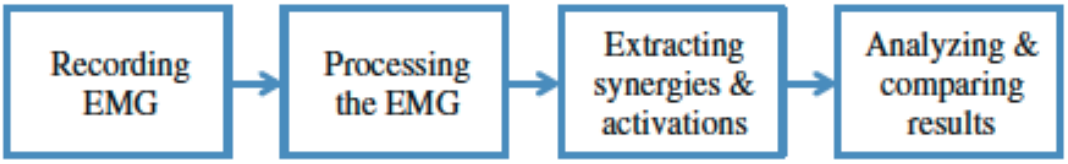

Figure 3.1: Block chain of the procedure for Muscle Synergies Extraction and Analysis [10]

Recording ElectroMyoGraphic signal

The procedure for the recording of sEMG signals has been previously explained in 1.2. It is necessary to record the sEMG signals with the highest quality possible, because the quality of the signals will influence the one of the extracted synergies. In this thesis, instead of collecting EMG signals or using previously recorded signals, sEMG signals have often been synthesized with procedures that will be explained in the following sections.

Processing the EMG

The sEMG signal needs to be prepared to be used as a input in the algorithms for the extraction of the muscle synergies. This process includes the cleaning of the signal from anything not related to the EMG activations, included all the different disturbs explained in section 1.2.2. To remove the noise and the disturbances, several successive operations of filtering are performed, with the final aim being the extraction of the envelope of the signal. Figure 3.2 shows an example of a sEMG signal acquired from the vastus lateralis muscle of a healthy subject during a cycling task going through the principal phases of processing.

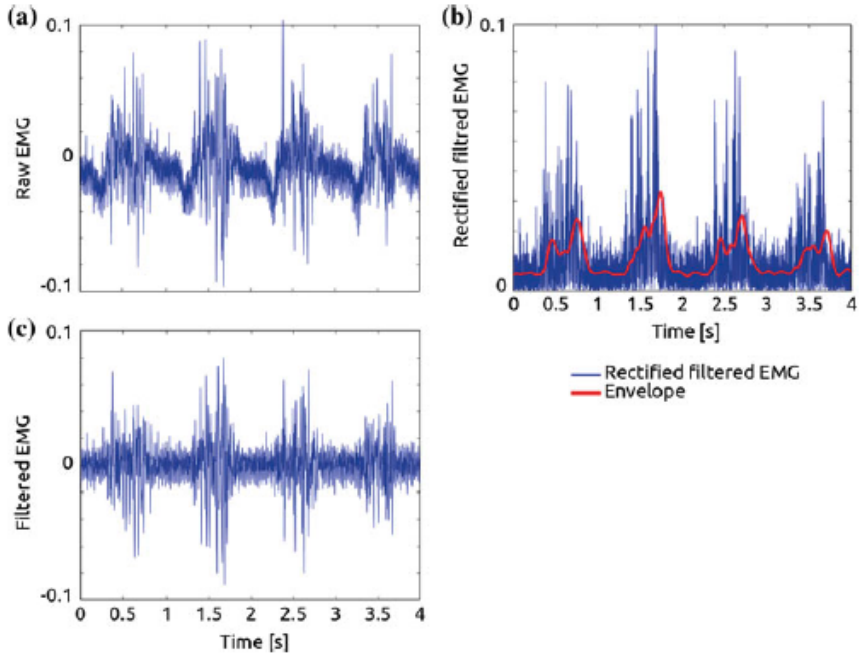

Figure 3.2: Processing of a sEMG signal to extract the envelope [10]. a) Raw EMG signal; b) Signal after band-pass filtering c)Blue: Rectified signal, Red: Envelope obtained after low-pass filtering

The graph in figure 3.2(a) shows the raw EMG signal, that is band pass filtered. The filter used in the thesis for this purpose is a Chebyshev Type I band pass-filter of the 5th order, with cutoff frequencies of 30Hz and 280 Hz and a band-pass ripple of 1dB. The low frequency cutoff frequency removes disturbs like motion artefacts and DC offset. On the filtered signal (figure 3.2(b)) is then applied a full wave rectification (figure 3.2(c), blue signal) and then a low pass filtering at 9 Hz, with a Chebyshev Type I filter of the 7th order and a band-pass ripple of 0.2 dB [44]. The final result of these operation is the envelope of the signal (figure 3.2(c), red

signal), a smooth curve that outlines the trend of the EMG signal. In some of the simulations performed in this thesis, instead of extracting the envelopes from EMG signals, they were directly synthesized to analyze the extraction of synergies independently from the influence of the noise of the signal on the extraction of the synergies, which is not completely removed when computing an envelope from a real EMG signal.

Extraction of Muscle Synergies

The basic functioning of the algorithms for the extraction of the synergies starting from the EMG signals, especially of the Non-Negative Matrix Factorization algorithm, has been detailed in section 2.3.1. To extract muscle synergies from the envelopes of the sEMG signals, the in-built function of MATLAB® *nnmf* has been used. The inputs required by the function are [45]:

- **sEMg envelope**: a matrix c x l, where c is the number of EMG channels analyzed and l is the length of every envelope.
- **k**: number of synergies to be extracted.

The outputs of the function are:

- **W**: a c x k matrix containing the extracted weights vectors for each synergy.
- **H**: a k x l matrix containing the temporal activations

The factors W and H are chosen by the algorithm to minimize the root-mean-squared residual between the input matrix and the reconstruction given by W*H. The factorization uses an iterative method starting from random initial values of W and H. The maximum number of iteration to perform can be set in the additional parameter **MaxIter**, which indicates the iteration where to stop if convergence has not been reached yet. In this thesis this parameter was set at 500.
Since the root-mean-squared may reach a local minimum, repeating the factorization could give different results. Sometimes the algorithm may converge to a solution with a rank lower than k. To get more stable results, the additional parameter **replicates**, which indicates the number of times to repeat the factorization using new random starting values for W and H, was set to 5000.
A crucial parameter to be given to the function is the number of synergies k. In section 2.3.1 some criteria for the choice of k have already been explained. During the different simulation performed in this thesis k has been chosen in different ways, so it will be explained in later sections for the corresponding simulations.

Analysis of the results

A first high level analysis of the synergies extracted can be performed by visual inspection. This can be carried out starting from the envelopes and checking some features like the presence of activation peaks, their number and their position, and the deviations from the average trend. When working with signals collected from a particular motor task, for instance the gait, the obtained synergies can be analyzed integrating them with physiological or biomechanics knowledge. For example, is very important to identify the muscles mainly activated for each synergy and their correspondent time activations, to contextualize the movement and observe its correspondence to the physiological movements.
To perform a qualitative and quantitative analysis of the performances of the algorithm extracting the synergies, various mathematical parameters can be computed:

- **Coefficient of Determination (R^2)**
  The coefficient of determination quantifies the linear correlation between the variability of the input data and the quality of the statistical model used to reconstruct it. In the case of the computation of muscle synergies, the input data is the matrix of envelopes of the signal, and the result of the model is the reconstructed envelopes with the results of the nnmf algorithm $W \times H$. This coefficient is calculated with the following formula [46]:

$$R^2 = 1 - \frac{SS_{res}}{SS_{tot}} \tag{3.1}$$

  where SS_{res} is the residual sum of squares (the sum of squares of the residuals) and SS_{tot} is the total sum of squares that is proportional to the variance of data.

$$SS_{res} = \sum_{i=1}^{n} (y_i - \hat{y}_i)^2 \tag{3.2}$$

$$SS_{tot} = \sum_{i=1}^{n} (y_i - \bar{y})^2 \tag{3.3}$$

  y_i are the original data, $\bar{y}$ is the mean of y_i, and $\hat{y}_i$ is the model estimation data. The maximum value that R^2 can assume is 1, meaning that the model has perfectly reconstructed the data.

- **Variance Accounted For** (VAF)
  It's a similarity metric used to quantify exact matches between two patterns, taking into account both shape and magnitude of the measured and reconstructed curves. [47] The VAF is often used to verify the correctness of a

model, by comparing the real output (original envelopes of the signal) with the estimated output of the model (envelopes reconstructed with nnmf). The formula used for the computation of the VAF between two signals is [48]:

$$VAF_i = 1 - \frac{var(y_i - \hat{y}_i)}{var(y_i)} \tag{3.4}$$

where *var* represent the variance of the data, y_i is the measured output (original envelopes of the signal) and $\hat{y}_i$ is the estimated output (envelopes reconstructed with nnmf). The maximum possible value for VAF is 1, meaning that the two signals are the same, the curves are perfectly matched.

- **Cosine Similarity**
  The Cosine similarity is a measure of similarity between two non-zero vectors. This index varies in the range between -1 and 1, but is generally used only in the positive range [0;1] respectively for absence of similarity and maximum similarity. The cosine similarity is used to compare the values of the weights of the synergies [49]. The cosine similarity was computed following the formula:

$$CS = \frac{W_i * W'_i}{||W_i|| * ||W'_i||} \tag{3.5}$$

- **Correlation Coefficient**
  The correlation coefficient, or cross-correlation, measures the similarity of two signals as a function of the displacement of one relative to the other, displacement that can be interpreted as a temporal shift. Zero-lag cross-correlation is a particular type of correlation in which the signals are compared with a zero delay. The correlation coefficient is used to compare the temporal activation vectors of the synergies. The formula for the cross correlation is [49]:

$$CC = \frac{R_{xy}[0]}{\sqrt{R_{xx}[0] * R_{yy}[0]}} \tag{3.6}$$

  There is an in-built MATLAB® function, *xcorr*, that compares the signals regardless of their amplitude. The zero-lag cross-correlation verifies if when one signal increases (or decreases) also the other increases (or decreases). The index varies in the range from 0 to 1, respectively for absence of similarity or total similarity.

Merging and fractionation analysis

As already discussed in 2.2, Cheung and others [11] studied muscle activation after lesions of the motor cortical area collecting EMG signals from upper-limb muscles in subjects with cortical lesions. Analyzing muscles synergies for the unaffected and the affected arm, three distinct patterns of muscle coordination in response to cortical damage were identified: preservation, merging and fractionation. This model can be adapted to the problem analyzed in this thesis, considering as *unaffected-arm synergies* the original generated synergies, in short *original synergies* and as *affected-arm synergies* the synergies obtained after the removal of one or more channels, in short *removed synergies*.

Model of Synergy Merging: each *removed* synergy is modeled as a linear combination of the *original* synergies:

$$\overrightarrow{w_i^r} \approx \sum_{k=1}^{N^o} m_k^i \overrightarrow{w_k^o}, \qquad m_k^i \geq 0, i = 1...N^r \tag{3.7}$$

where $\overrightarrow{w_i^r}$ is the ith removed synergy, $\overrightarrow{w_k^o}$ the kth original synergies, N^r the number of removed synergies, N^o the number of original synergies and m_k^i represents the contribution of the kth original synergy to the ith. For every removed synergy, an original synergy is defined to contribute to the merging if the associated coefficient is in the interval [0.3, 0.7] (a smaller interval than the original [0.2, 1] was considered). The merging coefficients are identified with nonnegative least square, implemented through the MATLAB® function *lsqnonneg*.

Model of Synergy Fractionation: each *original* synergy is modeled as a linear combination of the *removed* synergies:

$$\overrightarrow{w_k^o} \approx \sum_{i=1}^{N^r} f_i^k \overrightarrow{w_r^i}, \qquad f_i^k \geq 0, i = 1...N^o \tag{3.8}$$

where the coefficients $\overrightarrow{f^k} = [f_1^k, f_2^k, ...f_{N^a}^k]$ indicate how the kth original synergy may be fractionated into multiple removed synergies. As a first step, the fractionation coefficients $\overrightarrow{f^k}$ are identified without constraints applying the function *lsqnonneg*. For every removed synergy, the original synergy with the highest associated fractionation coefficient is identified, and it will be assigned to it as the only original one that may be reconstructed by that removed synergy. A second projection is performed, for every original synergy only onto the removed synergies assigned to it. A removed synergy is defined a fractionation only if the newly computed $\overrightarrow{f^k}$ indicated that it could be combined with another removed synergy to reconstruct one of the original synergies. The corresponding fractionation coefficient must verify the condition $\overrightarrow{f_i^k} > 0.2$.

3.2 sEMG envelopes simulations starting from synergies

The aim of this thesis was to evaluate the performances of the NNMF algorithm in extracting muscle synergies when one or more channels of the original signal are lost. Different simulation synthesizing the sEMG data to be used as input of the algorithm were performed.

In the first simulation, instead of generating a simulate version of a sEMG signal, extracting its envelope and performing the non-negative matrix factorization, it was decided to simulate directly the envelopes of a sEMG signal. This was done to avoid the influence of the typical noise in the sEMG signal, difficult to remove completely, on the reconstruction of the signal from the extracted synergies, and to focus only on the performances of the algorithm when channels are lost. To make so that the NNMF algorithm is faced with an exact factorization, the matrix containing the envelopes is generated starting from the muscle synergies, by multiplying two vectors, one representing the synergy weights and one the temporal activations: it is as if the envelopes computed were the envelopes reconstructed after the extraction of the synergies. For this reason, when muscle synergies are extracted from the generated envelopes it is expected that they would be equal to the original synergies that were generated
Indications on how to generate sets of vectors that could be assimilated as the synergy weight vectors or the temporal activations extracted from the sEMG were searched in literature. It was found that in [37] signals with characteristics similar to the one needed in this simulation were generated, and that the amplitude of those that can be considered the weight vectors was picked from the values of an exponential distribution with mean 10. From [50] it was taken the idea of *dominant muscles* (or dominant channels), defined as "muscles whose weight is within twenty percent of the maximum weight for each synergy": they represent channels that are particularly relevant in a synergy weight, since the amplitude of their corresponding weights it is significantly bigger than the amplitude of the weights for the rest of the channels. Starting from these two ideas, some criteria for the simulation of weight vectors and temporal activations, with the aim of generating a final envelope matrix of 12 channels starting from 4 synergies, were defined.

Weight vectors generation

- The amplitude of the single contribution: taken from an exponential distribution with average 10, in a different range for every categories of channels

(figure 3.4).

- In each synergies, 3 categories of channels were defined: *dominant semidominant* and *non dominant*. The *dominant channels*, inspired by the definition in [50], are the most relevant channels, and in every weight generated there must be between 2 and 5 of them. Two is set as minimum so that it is possible to see what happens in the algorithm when "important" channels are lost but at least one remains; five as maximum so that the four weight vectors generated are not too similar with each other. The amplitude of the dominant channels is selected randomly in the red range of the exponential distribution in figure 3.4. The *non dominant channels* are the channels that give only a small, almost null, contribution to the magnitude of the weight vector. Their number in a weight vector depends on the number of the channels belonging to the other categories, and their amplitude is taken from the green range in figure 3.4. The *semidominant channels* are a middle way between the other two categories, and their amplitude is picked from the yellow range in figure 3.4. They were introduced to have final weight vectors more similar to real possible weight vectors. Their number must be between 0 and 3.

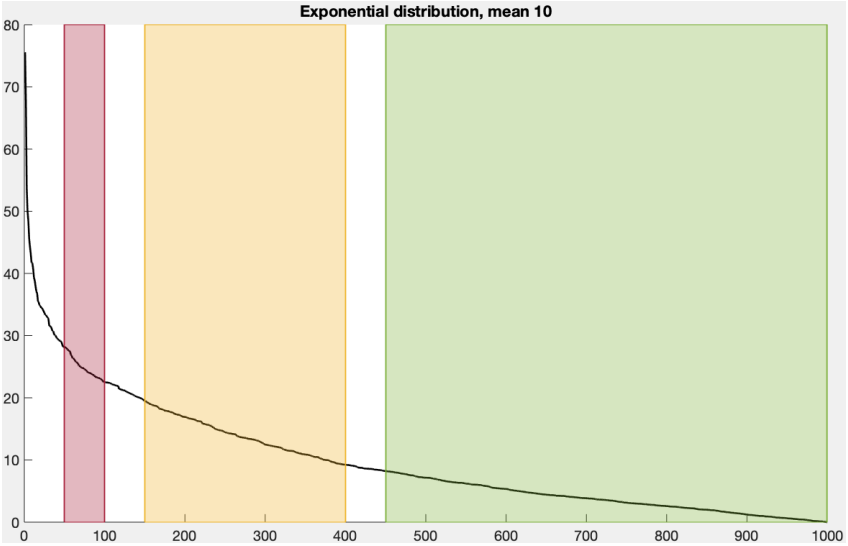

Figure 3.3: Range of values of an exponential distribution from where the amplitude of the three categories of channels is taken. Red zone: dominant channels. Yellow: semidominant channels. Green: non dominant channels.

- The minimum total number of dominant channels must be 15. The position of the dominant channels are assigned to every of the four synergies starting from a random distribution with no repetition of the values from one to twelve

and considering that for every channel there must be from 2 to 5 of them. When reaching the 13 dominant channel to assign, a new random distribution of the number from 1 to 12 is considered. In this way after the 12th channel it is possible to have a channel dominant for more than one synergy. The minimum number of dominant channels to be present in the set of 4 weight vectors was set at 3, so it is certain that at least 3 channels are dominant for more than one synergy. The maximum is set at 20 to not have synergies too similar between each other.

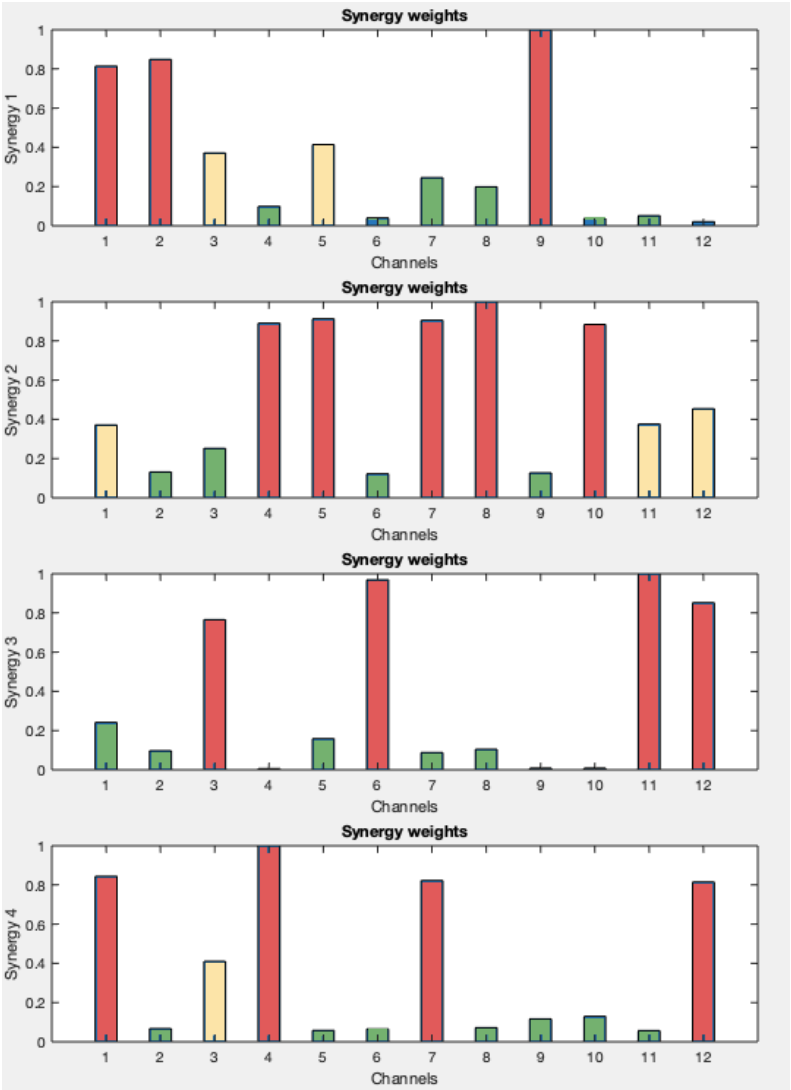

Figure 3.4: Example of a set of weight vectors. The dominant channels are highlighted in red, the semidominant in yellow and the non dominant in green.

- To avoid too similar synergies, that would make a successive factorization pointless, the cosine similarity between all the vectors was set to be lower than 0.7

Temporal activations generation

- 4 Gaussian functions, 1000 samples long

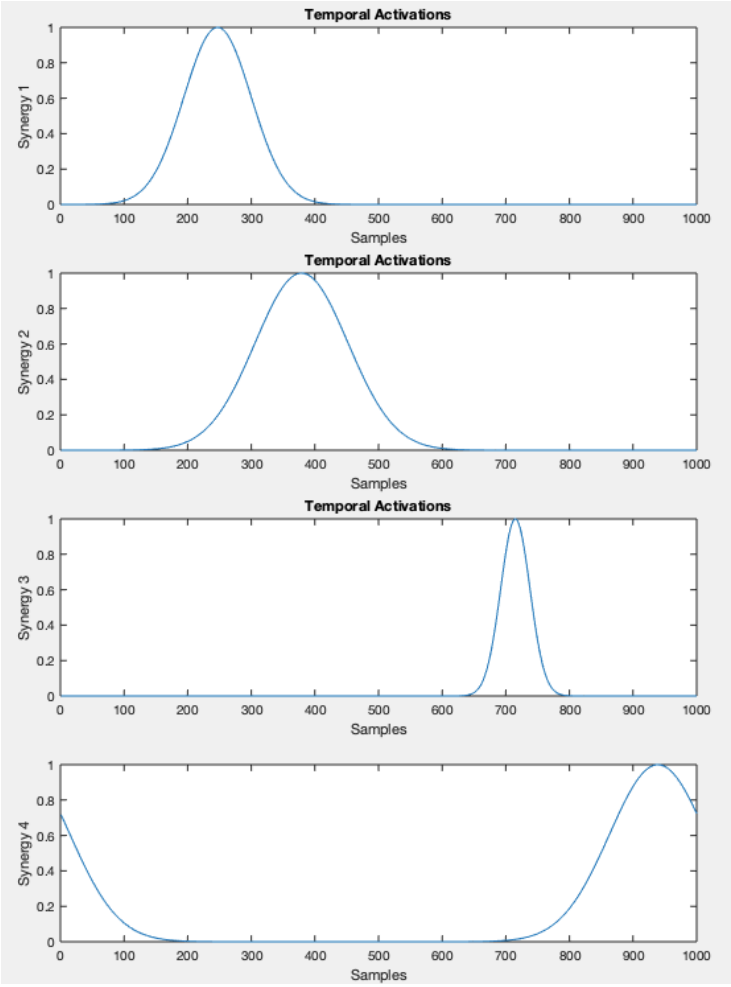

Figure 3.5: Example of a set of temporal activations

- To avoid having four overlapping functions, intervals for the σ, the standard deviation of the Gaussian distribution, and for the μ, the mean value, are selected. The interval for σ is the same for the four activations: $20 < \sigma < 100$. The average values of the four gaussians were selected from four adjacent intervals: $0 < \mu_1 < 250$, $251 < \mu_2 < 500$, $501 < \mu_3 < 750$ and $750 < \mu_4 < 1000$

After generating a 12x4 matrix containing the four weight vectors (W) and a 4x1000 matrix containing the four temporal activations (H), the simulated envelope is obtained from their product, and it will have dimensions 12x1000.
From the generated envelope, we start the simulation, removing channels as explained in figure 3.6. At the beginning, the envelope has 12 channels. One channel

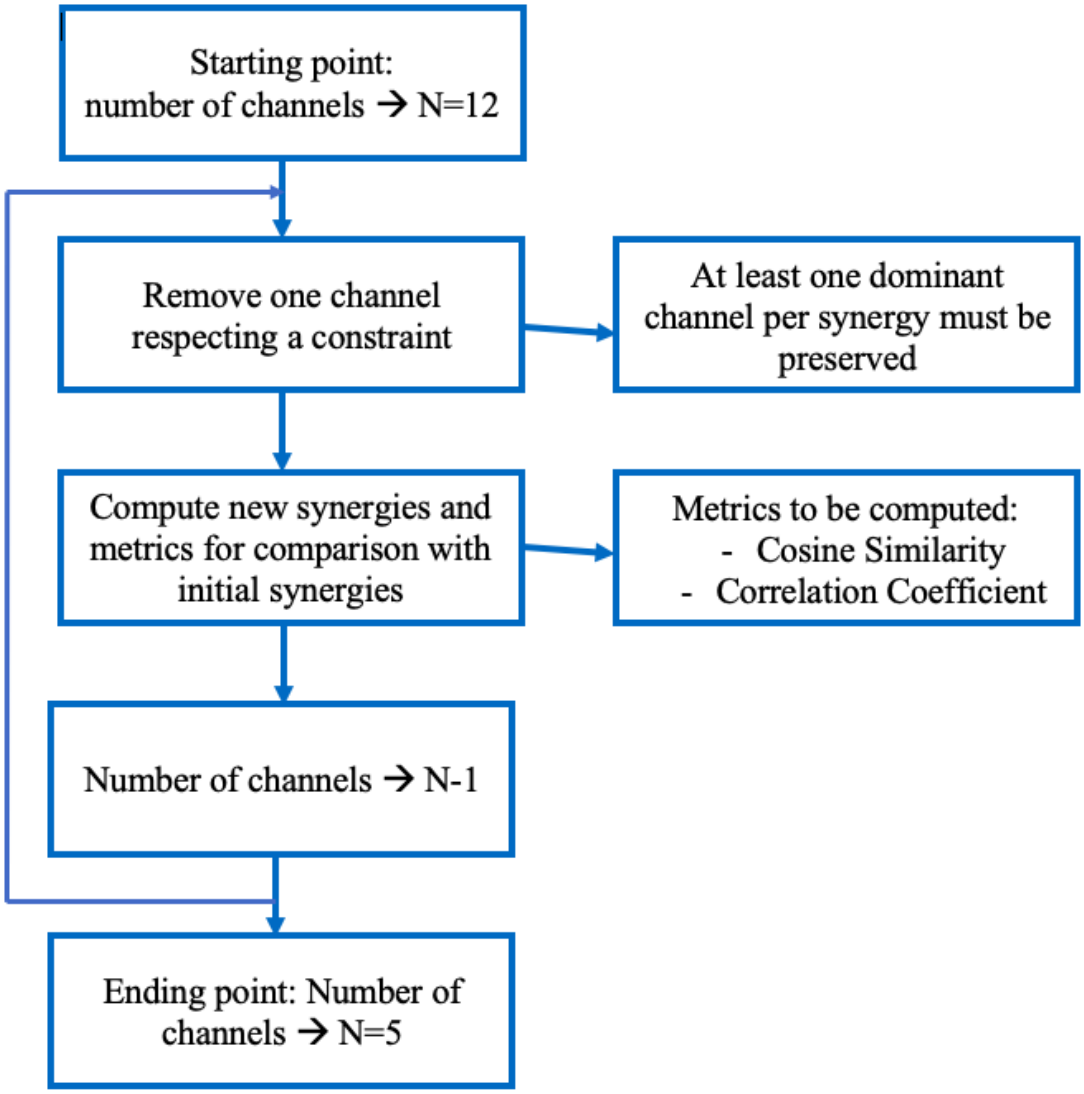

Figure 3.6: Block diagram describing the main loop of the performed simulation

is removed, choosing it randomly but making sure that it satisfies the condition that even after its removal there is still at least one dominant channel for every synergy. Then, new synergies are extracted from the envelope with the new number of

channels, and they are compared with the original generated synergies computing the Cosine Similarity between the weight vectors and the Correlation Coefficient between the temporal activations. In this simulation, the number of synergies extracted has been kept fixed to 4, as the original synergies that were generated. Since, in this case, an exact factorization is performed by the algorithm, to better evaluate its performances it is necessary to keep the number of synergies fixed, to see how its performances change as more channels are lost. The removal of the channels and the consequent computation of synergies and metrics continues until the number of channels reaches five: the stopping point is set here because the loss of another additional channel would lead to the loss of one synergy.

3.3 sEMG signal simulations

In the second set of simulations, the signal considered was no longer only the envelope of an sEMG, but it was a simulated sEMG signal. Signals with different noise contribution were generated, to observe the effect of the noise on the performances of the algorithm. To generate a sEMG signal it was used a procedure illustrated in [12].

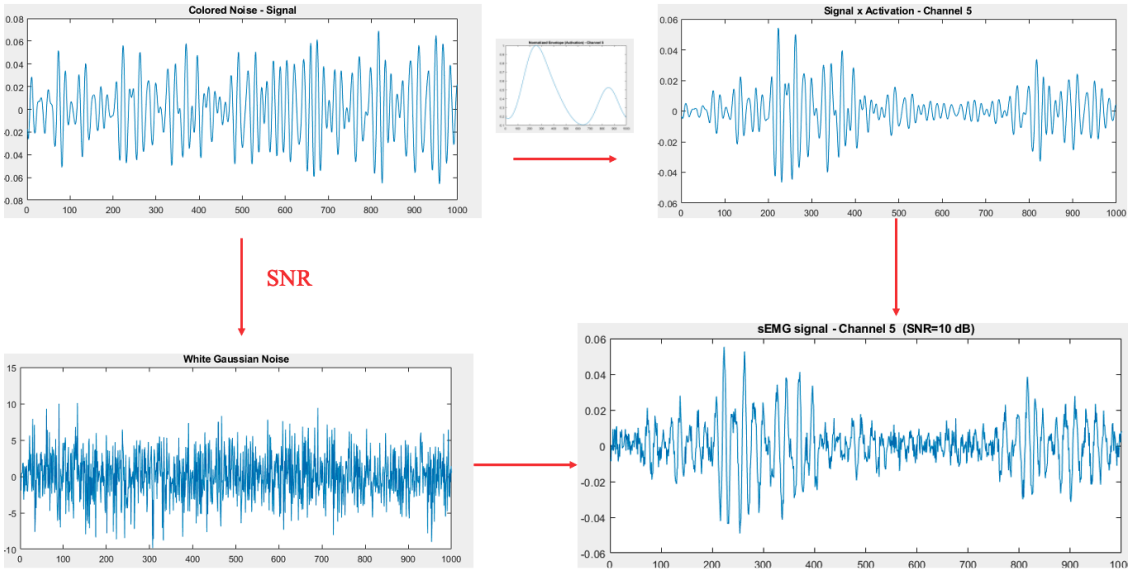

Figure 3.7: sEMG generation process: starting from the colored noise in the top left, in the bottom left it is plotted the generated white noise, in the top right is shown the "pure" signal obtained by multiplying the colored noise by the activation. Finally, in the bottom right the sum of these two last signals gives the final simulated sEMG signal

The first step is the creation of a white noise signal with a certain power. This signal is then filtered with a band-pass filter to leave only the frequency components in the range of interest.

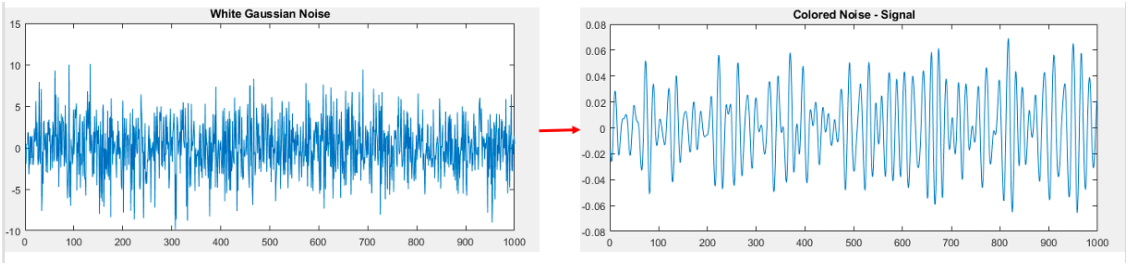

Figure 3.8: First Step: extraction of a Colored Noise Signal by filtering of a White Gaussian Noise

The lower boundary of the frequency interval that has been considered is 40 Hz, and the upper boundary is 80 Hz: according to [51] this is the most informative band of the power of the sEMG signal.
The second step consists in the generation of a new white noise signal that will represent the noise part of the final sEMG. Starting from the power content of the colored noise previously obtained, this new white noise is generated according to a desired SNR value. The power of the noise to be created is obtained inverting the

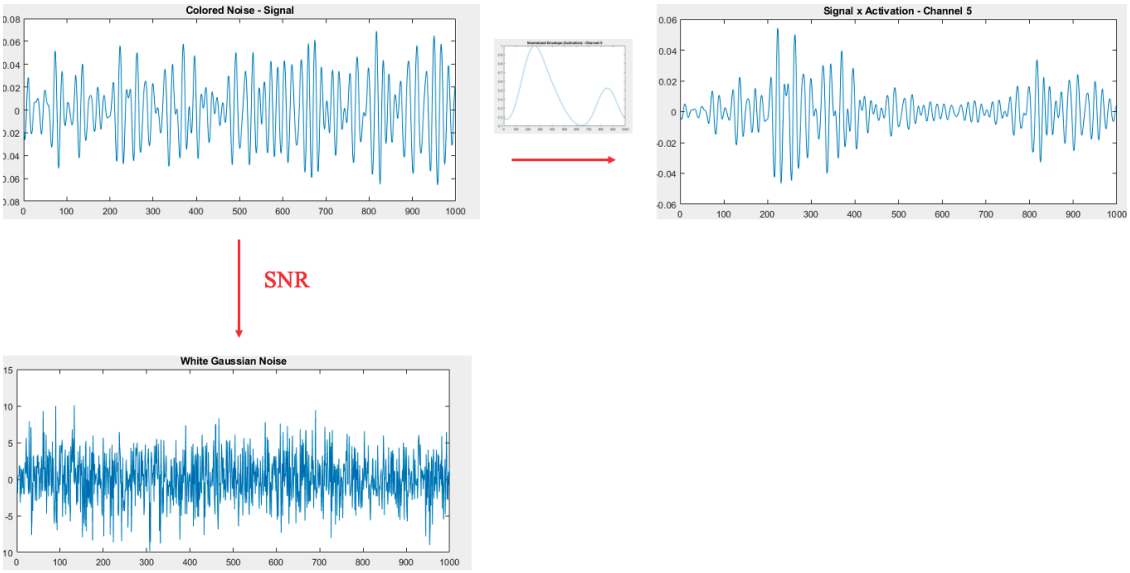

Figure 3.9: Second Step: Noise and Signal components generation

formula for the signal-to-noise ratio:

$$SNR_{dB} = 10 \log \frac{P_s}{P_n} \tag{3.9}$$

In the simulation, five different values of SNR were tested to observe the performances of the algorithm with its variation. The values are 0 dB, 5 dB, 10 dB, 15 dB and 20 dB. In the same step, the colored noise is multiplied by a function that delineates the profile of the activity of the muscle. The envelopes obtained from the product of the sets of weights and temporal activations have been used as activation function for the modulation of the sEMG.
The final step consists in the sum of the white noise of a certain SNR and the result of the product of the colored noise with the activation.

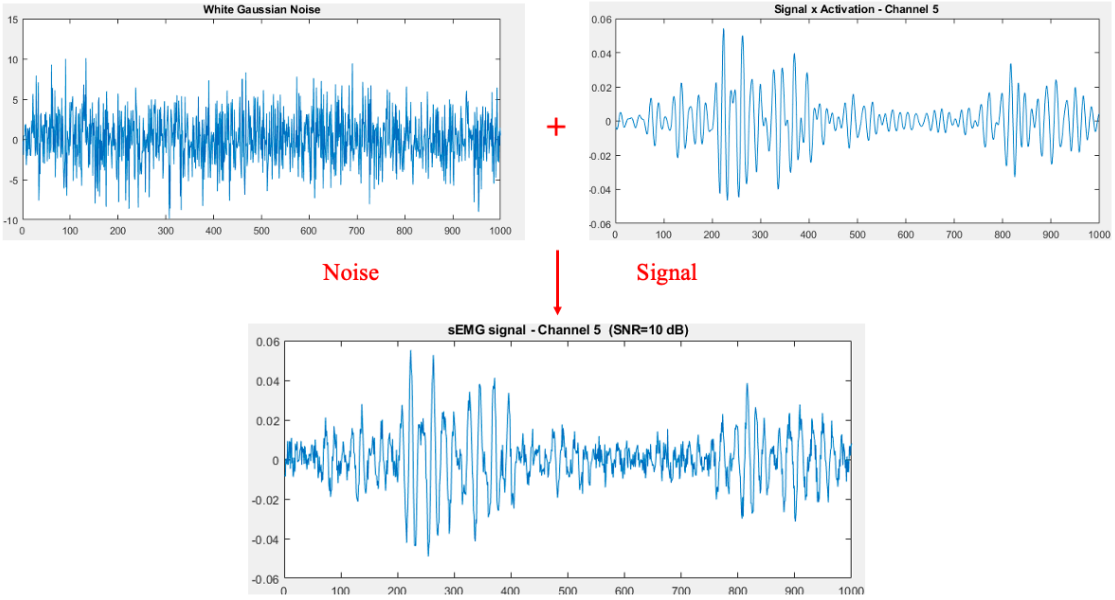

Figure 3.10: Final Step: Generation of a sEMG signal with a noise of 10 dB by sum the Noise and the Signal components

Once the signals are generated, in order to be used for the extraction of the sEMG signal they must be processed for the extraction of their envelopes. This happens following the steps indicated in 3.1. From this point on the simulation follows the same main loop of the previous one, removing one channel at a time pseudo-randomly and evaluating the performances of the algorithm by comparing the synergies after the removal of channels with the synergies that are obtained from the sEMG signals generated. Also, in these simulation the number of synergies was kept fixed to k=4.

3.4 sEMG envelopes simulations starting from the synergies: shifting of the original envelopes

In this bunch of simulations, the starting point was again the envelopes of the sEMG signal rather than the complete signal. However, to have some variability, a new parameter in the generation of the temporal activations was introduced. The coefficient δ is added to the Gaussian parameters σ and μ to shift the profile of the Gaussian: δ is randomly picked in the interval [-15,15] and it is different for every simulated Gaussian. In the simulation in section 3.2 the envelopes were all generated in the same step using the same temporal activations, resulting in a 12x1000 matrix obtained by the multiplication of the 12x4 weight matrix with the 4x1000 temporal activations. In these simulations, the envelope of each channel is computed individually, considering the contribution of the channel to the weight matrix (a column of the matrix, so a 1x4 vector) and multiplying it for a set of 4 temporal activations (a 4x1000 matrix). The temporal activations will be slightly different for every channel, because for every channels different values of δ are added to the σ and μ of the set of 4 Gaussians originally generated and set as a reference. An example of a set of envelopes generated in this way, compared with the original envelopes that would have been obtained if the parameter δ was not introduced, is reported in figure 3.11.

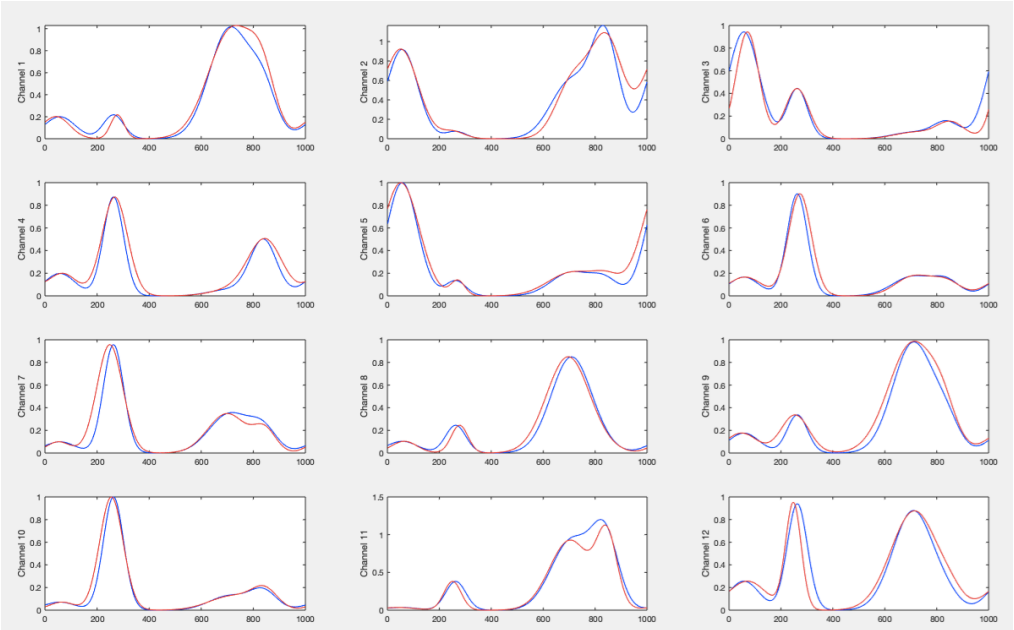

Figure 3.11: Comparison between the original envelopes (blue) and the envelope obtained shifting the temporal activations (red)

It is important to select the range in which δ can vary in a way that the "shifted" envelopes will not be too different from the original ones so that the NNMF algorithm would still be able to reconstruct them with results not too different from the original set of synergies (with the reference temporal activations). To verify that [-15,15] was a good enough interval for δ, the correlation coefficient between the original envelopes and the shifted envelopes was computed (figure 3.12).

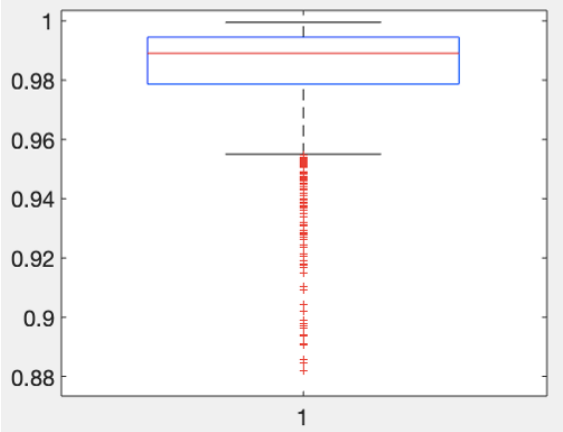

Figure 3.12: Distribution of the correlation coefficient between the original and the shifted envelopes

The main loop of the simulation (figure 3.13) is slightly different from the one of the initial simulation presented in section 3.2. In that case, since the envelopes were given exactly by the product of the W and the H used as reference, the algorithm was performing an exact factorization, so the number of synergies to be extracted was set as 4 and kept constant across all the channel removals to compare the synergies extracted after the loss of channels with the original generated synergies. In this simulation, shifting the envelopes introduces variability, so reconstructing the signal through the NNMF algorithm is no longer an exact factorization, but a pseudo factorization. For this reason, it was decided not to keep the number of synergies k a priori fixed to 4, but to choose it extracting the synergies at the beginning from the shifted envelopes (when having all the 12 channels) and to keep it constant across the removal of channels. The criteria for the selection of k were chosen from literature [11]: the synergies were extracted with different values of increasing k, the coefficient of determination R^2 was computed between the original envelopes and the reconstructed envelope for every possible k, and it was picked the first value of k for which the average R^2 was higher than 0.85, and the R^2 for every channel was higher than 0.70.
Once the optimal value of k was picked, it was kept fixed across the consecutive

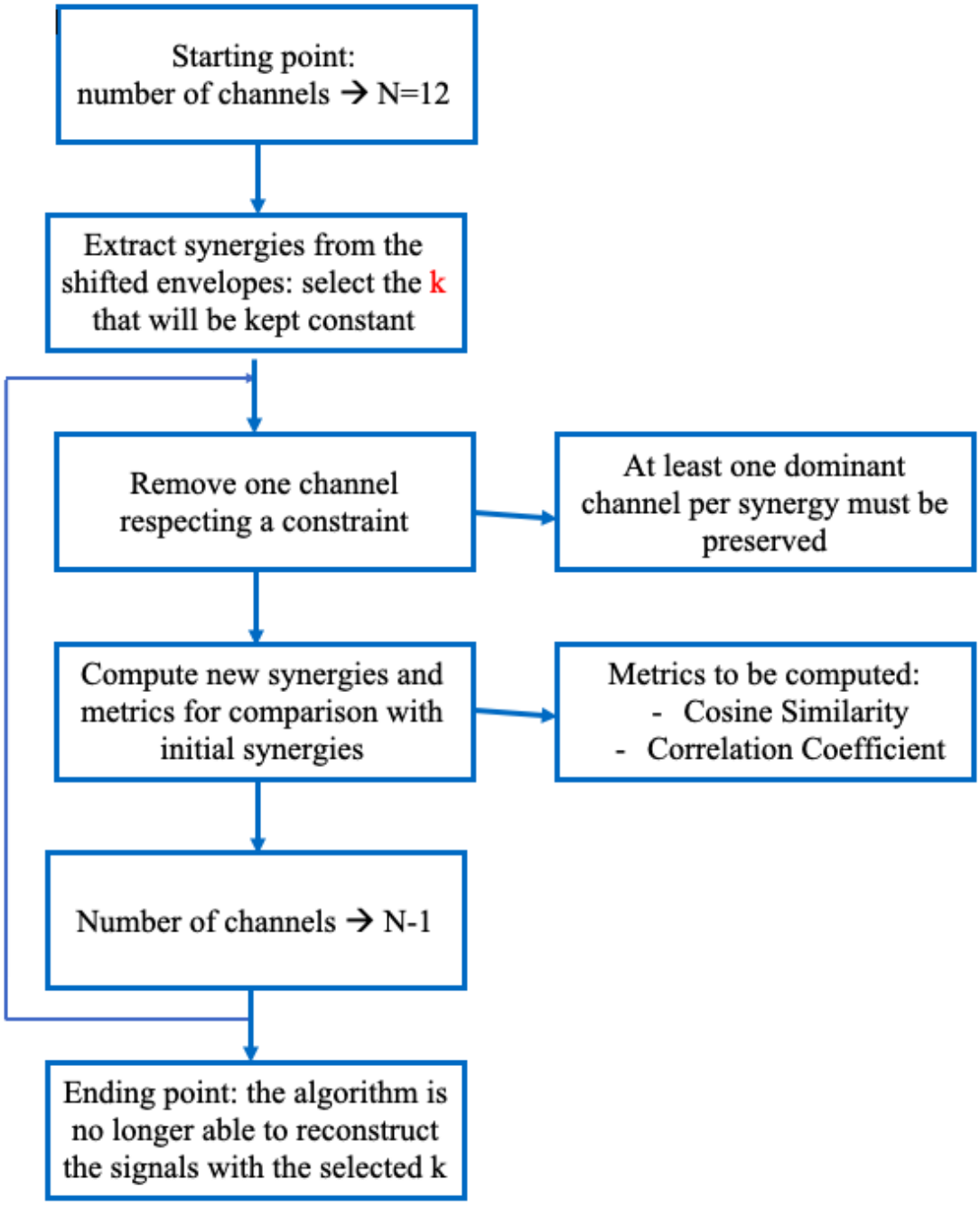

Figure 3.13: Block diagram describing the main loop of the performed simulation

removals of channels. The ending point of the simulation was also different from the one of the previous one: the simulation was stopped when the algorithm was no longer able to reconstruct the signals of the remaining channels with the same

number of k initially picked.

3.5 sEMG simulations starting from physiological activations

To test the algorithm in conditions as similar as possible to physiological ones, a simulation was performed focusing on data from the gait analysis. The gait is a highly repeatable task, and the study of EMG signals collected from the muscles involved allows to evaluate pathological conditions by studying the activations of the muscles and the synergies patterns.
In literature, gait analysis is a theme widely explored, as it is the application of muscle synergies to it, so it was possible to find some activity patterns of muscles during gait and replicate it. In particular, it was considered the averaged EMG activity collected from 25 muscles from 18 subjects during a cycle of over-ground locomotion (reported in [14]).

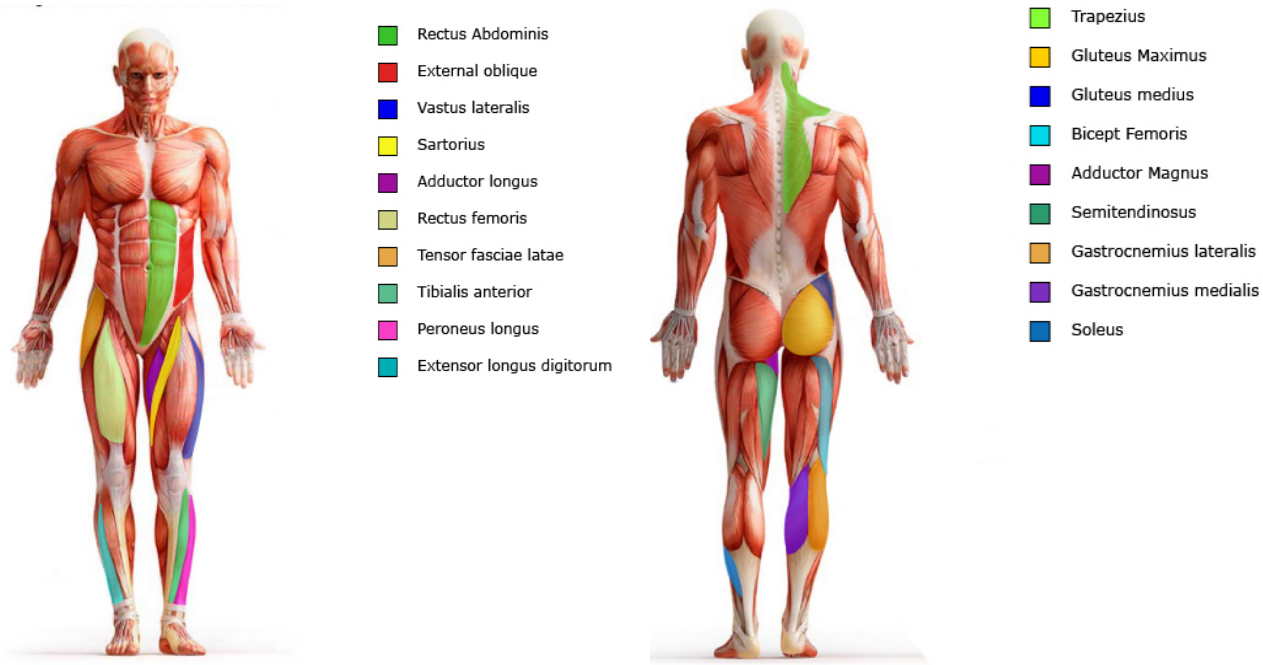

Figure 3.14: Anterior and Posterior view of the muscular system: some of the muscles considered in the analysis are highlighted (adapted from [13])

The position of most of those muscles in the human body is shown in figure 3.14.

Channel	Muscle	
1	Adductor longus	ADDL
2	Adductor magnus	ADDM
3	Biceps femoris	BF
4	Extensor digitorum longus	EDL
5	Erector spinae lumbar	ES(L4)
6	Erector spinae thoracic	ES(T9)
7	Gastrocnemius lateralis	LG
8	Gastrocnemius medialis	MG
9	Gluteus maximus	GM
10	Gluteus medium	Gmed
11	External oblique lateralis	OEL
12	External oblique medialis	OEM
13	Peroneus brevis	PERB
14	Peroneus longus	PERL
15	Rectus abdominus	RA
16	Rectus femoris	RF
17	Sartoriys	SART
18	Semitendinosus	ST
19	Soleus	Sol
20	Splenius	SPLEN
21	Tibialis anterior	TA
22	Tensor fascia latae	TLF
23	Trapezius	TRAP
24	Vastus lateralis	VL
25	Fifth metatarso-phalangeal joint	VM

Table 3.1: List of the 25 muscles whose EMG was replicated

The data were manually digitized from the graphs in figure 3.15, selecting around 30 points per graph, interpolating and then re-sampling to have signals 1000 samples long. The result is reported in figure 3.16.

Considering those activations as EMG envelopes, muscle synergies were extracted from the digitized data (figure 3.17). The number of synergies obtained was 5, the same as the one that was obtained in [28] in a study analyzing the muscle synergies obtained from gait.

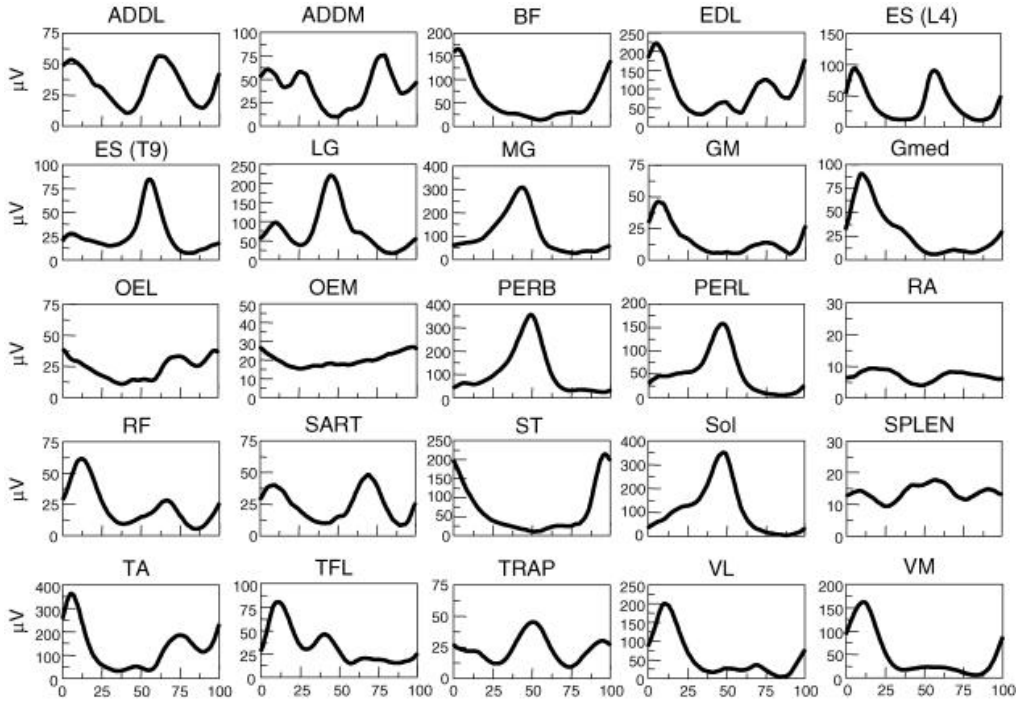

Figure 3.15: Activity patterns during a single locomotion step cycle ([14])

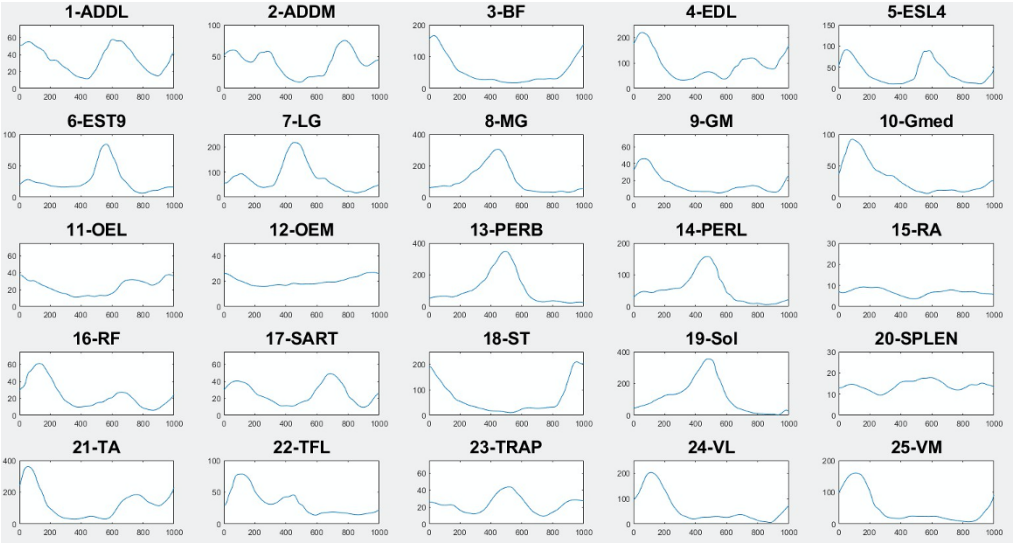

Figure 3.16: Activity patterns during a single locomotion step cycle - digitized data

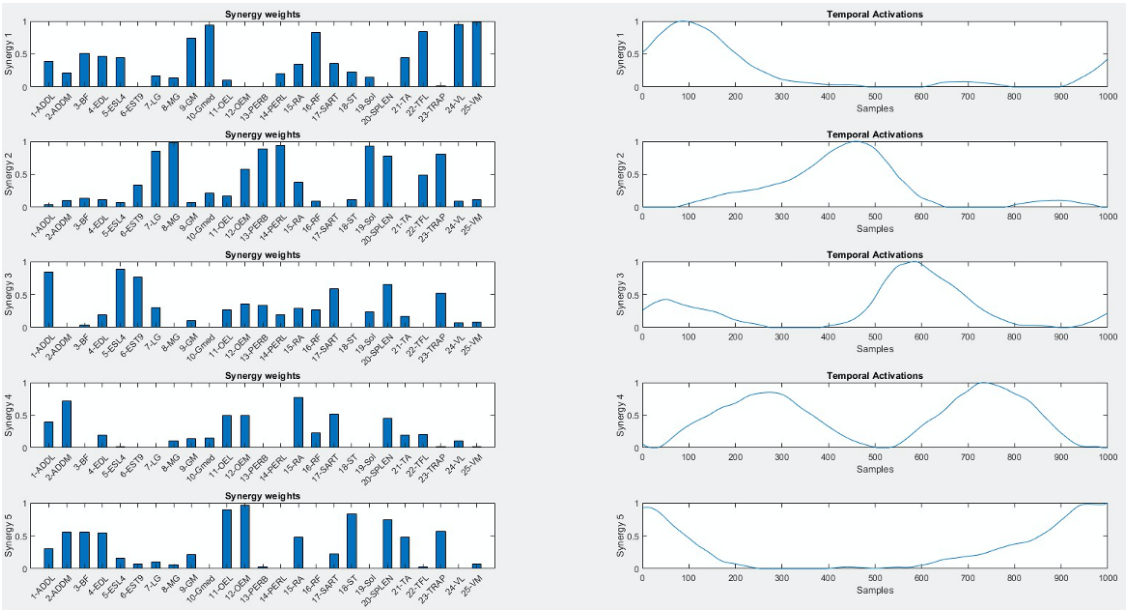

Figure 3.17: Initial synergies extracted

The main loop of the simulation (figure 3.18) is slightly different from the one of previous simulations. Also in this simulation as in the first one, the number of synergies was kept fixed to 5, that has been observed many times as the ideal number of synergies for signals from the gait analysis.
Every time a channel had to be removed, at first the removal of all the remaining channels was tested, computing every time the new synergies and the metrics for comparison with the original synergies (Cosine Similarity for the weights and Cross Correlation for the temporal activations). The choice of the channels to be removed followed two parallel patterns. In the first one, the channel that was removed was the one whose removal would less affect the performances of the algorithm,i.e. the channel for whom the synergies after its removal were more similar to the original synergies. In the second pattern, the channel that was removed was the one whose loss would most reduce the performances of the algorithm (while still satisfying the criterion that for every synergy at least a dominant channel must remain, to avoid losing that synergy). Every time a channel had to be removed, the same logic was applied. The simulation stopped when the number of channels left was 6, one more of the computed 5 synergies.
Following this approach, it was possible to analyze the best and the worst case scenarios for the loss of channels in this physiological signals, and it can be assumed that all the behaviours in between are possible.

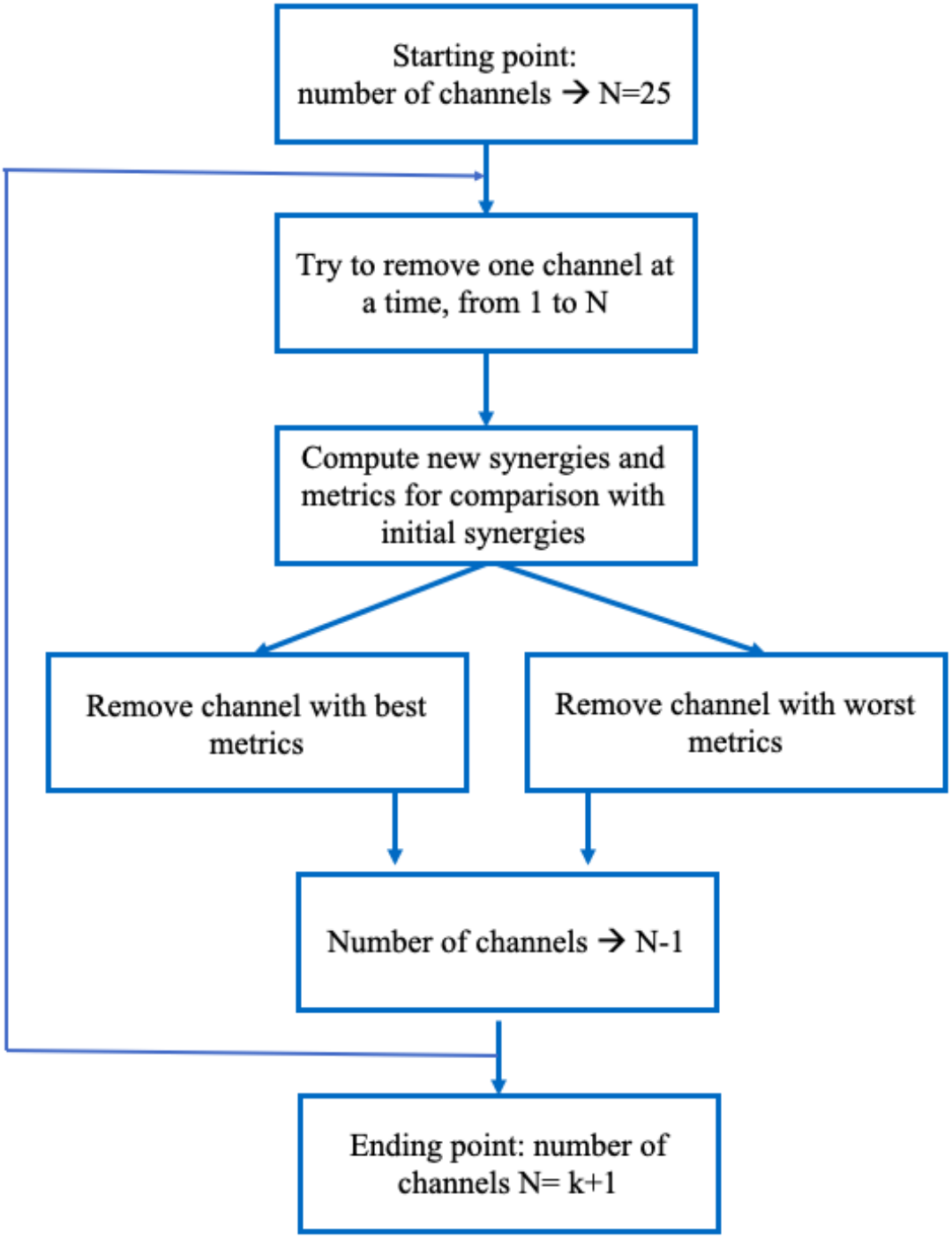

Figure 3.18: Block diagram describing the main loop of the performed simulation

Chapter 4

Simulations results and discussion

4.1 sEMG envelopes simulations starting from synergies

The simulation of the sEMG envelopes starting from the original synergies was performed 1000 times, 1000 different set of synergies were generated and were used as starting point for the successive removal of channels as described in figure 3.6. To observe how the algorithm reacts to the loss of the channels, the cosine similarity and the correlation coefficient are computed after every removal between the new extracted synergies and the original generated synergies. The distribution of the

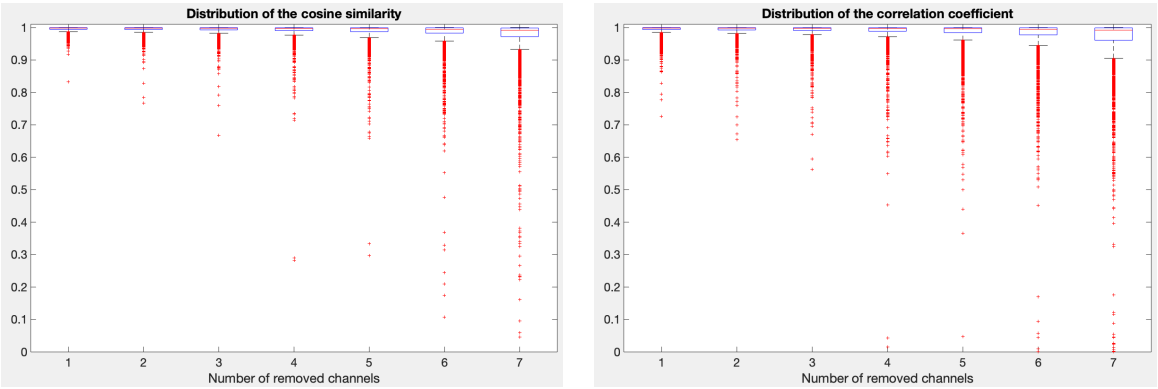

Figure 4.1: Distribution of the cosine similarity (left) and the correlation coefficient (right) between the synergies after the removal of channels and the original synergies as the number of removed channels increases

cosine similarity and the correlation coefficient as the number of channels decreases is reported in figures 4.1 and 4.2. The x axis reports the number of channels that

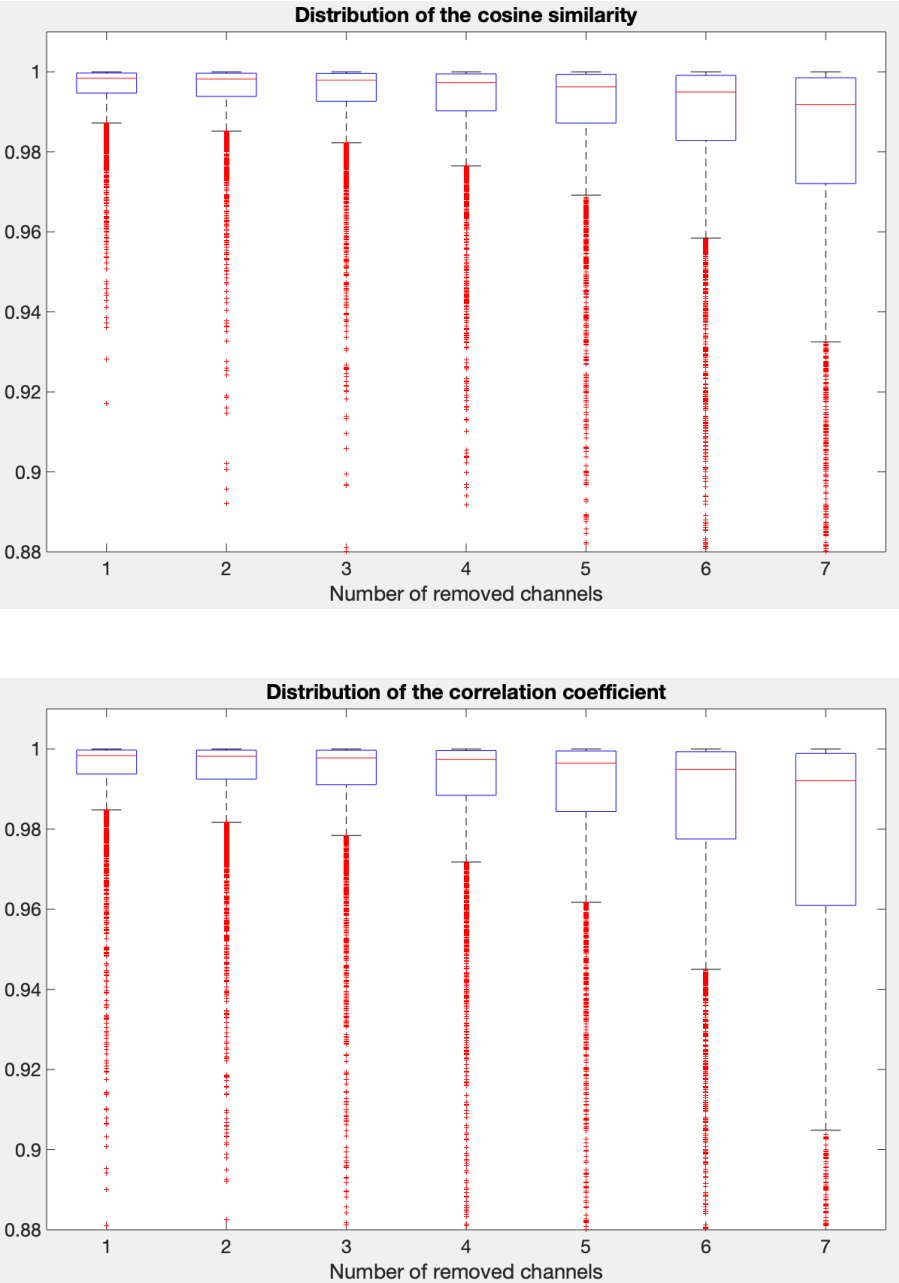

Figure 4.2: Distribution of the cosine similarity (up) and the correlation coefficient (down) between the synergies after the removal of channels and the original synergies as the number of removed channels increases.

have been lost, the y axis the values of the two parameters.

From the two graphs it is possible to observe that the average values for both cosine similarity and correlation coefficient are really high, greater than 0.98. A similar result is expected, since in this simulation the algorithm is faced with an exact factorization. The performances of the algorithm are influenced by the redundancy of the channels: there may be channels whose contribution to the weight vectors are really similar. The removal of a redundant channel would not affect the amount of information, and this may lead the algorithm to a different reconstruction with respect to the original reconstruction, and thus to lower values for the metrics of comparison.

Analysis of the outliers

It can be observed from the previous boxplots that there is a consistent number of outliers, spread out over a large interval of values. In looking for an explanation for their behaviour, three categories with common patterns in their behaviour were found.

- **Outliers with one of the synergies that is almost empty**
  These outliers were identified by computing the norms of the weight vectors and selecting the tests where one of the weights had a norm minor than 0.5. An example of an outlier in this group is represented in figure 4.3. In the upper part of the figure there are the original generated synergies with 12 channels, in the bottom part of the figure the synergies obtained after the removal of 7 channels. The dominant channels for the various synergies are colored in red, while the blu channels are semidominant or non dominant channels. It catches soon the eye that the third synergy has norm almost null: the synergy is almost void, also the last visible channel, that being a dominant channel and the only dominant channel left in the synergy was supposed to be remain sufficiently high, is almost null.
  It was observed that these outliers are linked to the fact that the number of synergies was kept fixed to k=4. To compensate this, in situations where k=3 would have been an appropriate number of synergies, the algorithm was oriented toward that optimal factorization, and, to get a result as close as possible to it, then one of the synergies was left empty so that its influence is null in the reconstruction of the envelopes. This has been proven true computing the R^2 coefficient of these outliers for a k=3 : the value was still very high (average of 0.99), so it would have been possible to reconstruct the signals also with k=3.

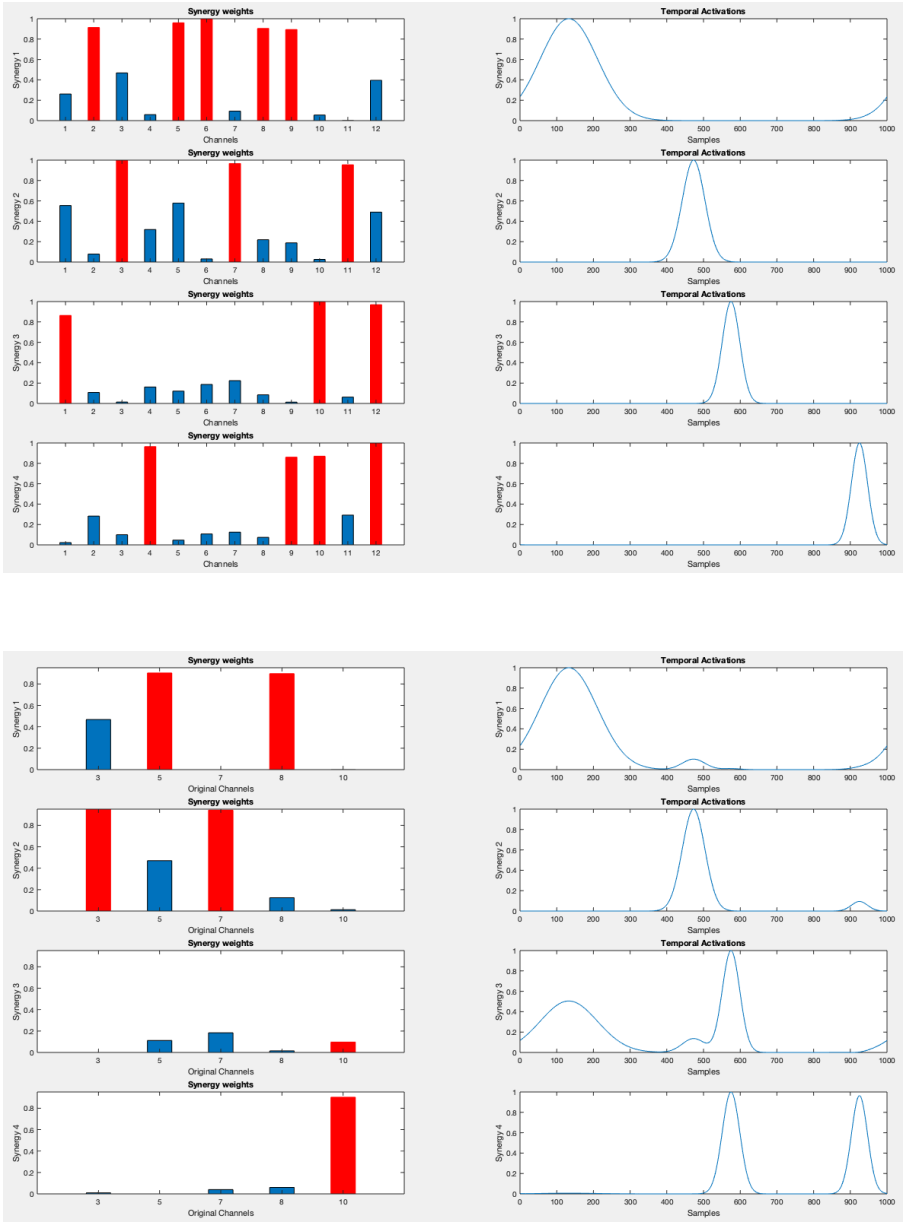

Figure 4.3: Synergies obtained from the original 12 channels (up) and from 5 channels (down): the test is an outlier and one of the synergies disappears. The channels highlighted in red are those who were dominant channels at the beginning of the simulation.

- **Outliers where one of the synergies after the removal of channel is given from a merging of two or more original synergies**

  These outliers were identified performing the merging analysis explained in section 3.1. Because of the presence of merging, one of the synergies obtained

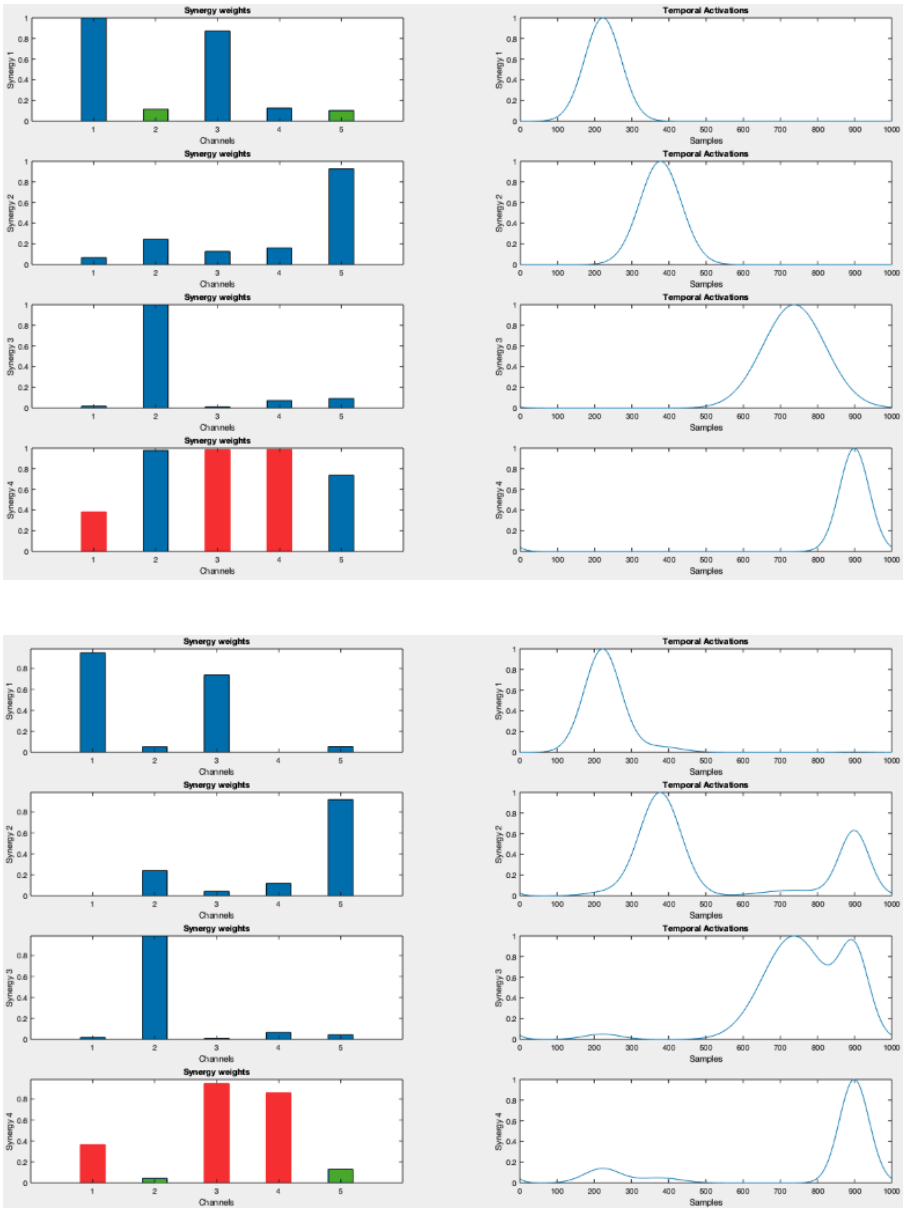

Figure 4.4: Example of an outlier where one of the synergies after removing channels could be considered as the merging of two of the original synergies. In the upper figure there are the original synergies, while in the lower the reconstructed synergies. The red channels are the ones that the 4th removed synergies has taken from the 4th original synergy, while the green are those taken by the 1st original synergy.

after the removal of channels can be obtained by merging two of the original synergies (considering for the comparison only the correspondent channels that are left). In this way, the new synergies result to be different from the corresponding original ones, that's why the tests where merging was detected were almost all part of the outliers. In figure 4.4 a possible example of merging is reported. In this case the 4th synergy obtained after the removal of 7 channels could be interpreted as the merging of the 4th original synergy (from which it has taken the channels 1, 3 and 4) and of the 1st original synergy (from which it has taken the channels 2 and 5).

- **Outliers where two or more of the synergies after the removal of channels are given from a fractionation of an original synergy**
  These outliers were identified performing the fractionation analysis explained in section 3.1. The idea is the same as the merging, but in the opposite direction: the original synergies are broken up and generate the reconstructed synergies. The individuation of a fractionation is more difficult than the one of the merging, because an additional constraint must be introduced: each removed synergy can contribute to the reconstruction of at most one original synergy, therefore the optimization algorithm must be implemented twice. Because of this difficulty, the number of outliers belonging to this category is low, lower than the number of elements belonging to the other categories. In figure 4.5 we can see an example of fractionation. The 3rd and 4th synergies after the removal of 7 channels derive from the fractionation of the 3rd original synergies.

A big chunk of the outliers of the test are part of one of the three categories, though not all of them.

A point that needs to be highlighted is the fact that the synergies provided by the NNMF in case of the outliers are, in most cases, still valid synergies and they provide a good reconstruction of the original signal, it is just that they are different from the originally generated synergies. Since the number of synergies is fixed to 4, it may happen that the algorithm has too much freedom in exploring the solution space and ends up computing synergies different from the original ones.

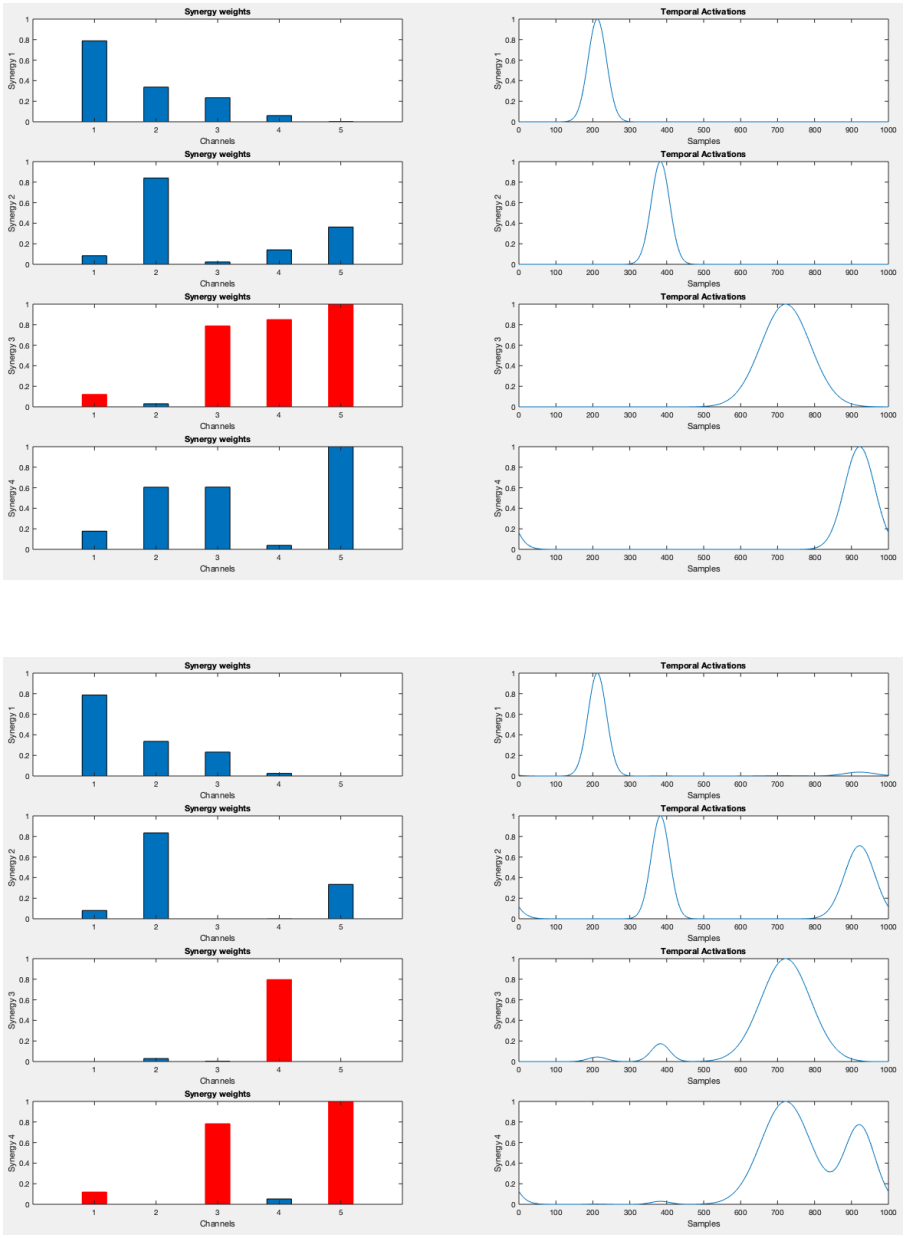

Figure 4.5: Example of an outlier where two of the synergies after removing channels are given by the fractionation of one of the original synergies. In the upper figure there are the original synergies, while in the lower the reconstructed synergies. The highlighted channels are the one involved in the fractionation: the 3rd original synergy is split in the 3rd removed (the contribute of the original synergy is channel 3) and the 4th removed synergy (the contribute consists in channels 1, 3 and 4)

4.2 sEMG signal simulations

The simulations with a sEMG signal as starting point were performed for 5 different values of the SNR: 0 dB, 5 dB, 10 dB, 15 dB and 20 dB.
To observe the influence of the SNR in the reconstruction of the original signal through the NNMF as the number of channels decreases, the results for the cosine similarity and the correlation coefficient were compared across the five intensities of the noise (figures 4.6 and 4.7).

The x axis indicates the number of channels that have been lost. The starting

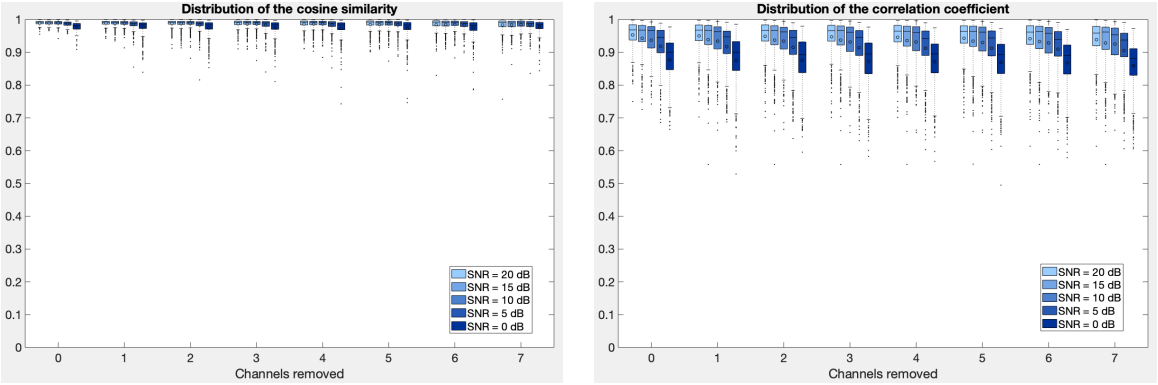

Figure 4.6: Distribution of the cosine similarity (left) and the correlation coefficient (right) between the synergies after the removal of channels and the original synergies as the number of removed channels increases: comparison for the different values of the SNR

point is 0 because the extraction of the synergies is performed from the original signal also before starting with the removal of channels: since the signal is affected by noise, it will not be reconstructed exactly, but, as reported in the graph, the synergies that are extracted are still very similar to the original generated synergies. In every column of the boxplot it is possible to observe the distribution of the analyzed parameters across the different values of SNR, starting from the left with the lightest blue from the signals with less noise/higher SNR (20 dB), from left to right the SNR decreases/the noise increases until the maximum value of 0 dB. As the noise increases, the capability of the algorithm to reconstruct synergies similar to the original ones decreases. Regarding the cosine similarity, the values are still high (average above 0.97), but the correlation coefficient has lower values. This is because, being the correlation coefficient related to the temporal activations, it is more affected by the SNR ratio than the weight vectors, since also the noise is time-dependant. Although in this simulation some outliers are present, they have values of cosine similarity and cross correlation which are still quite high (mostly

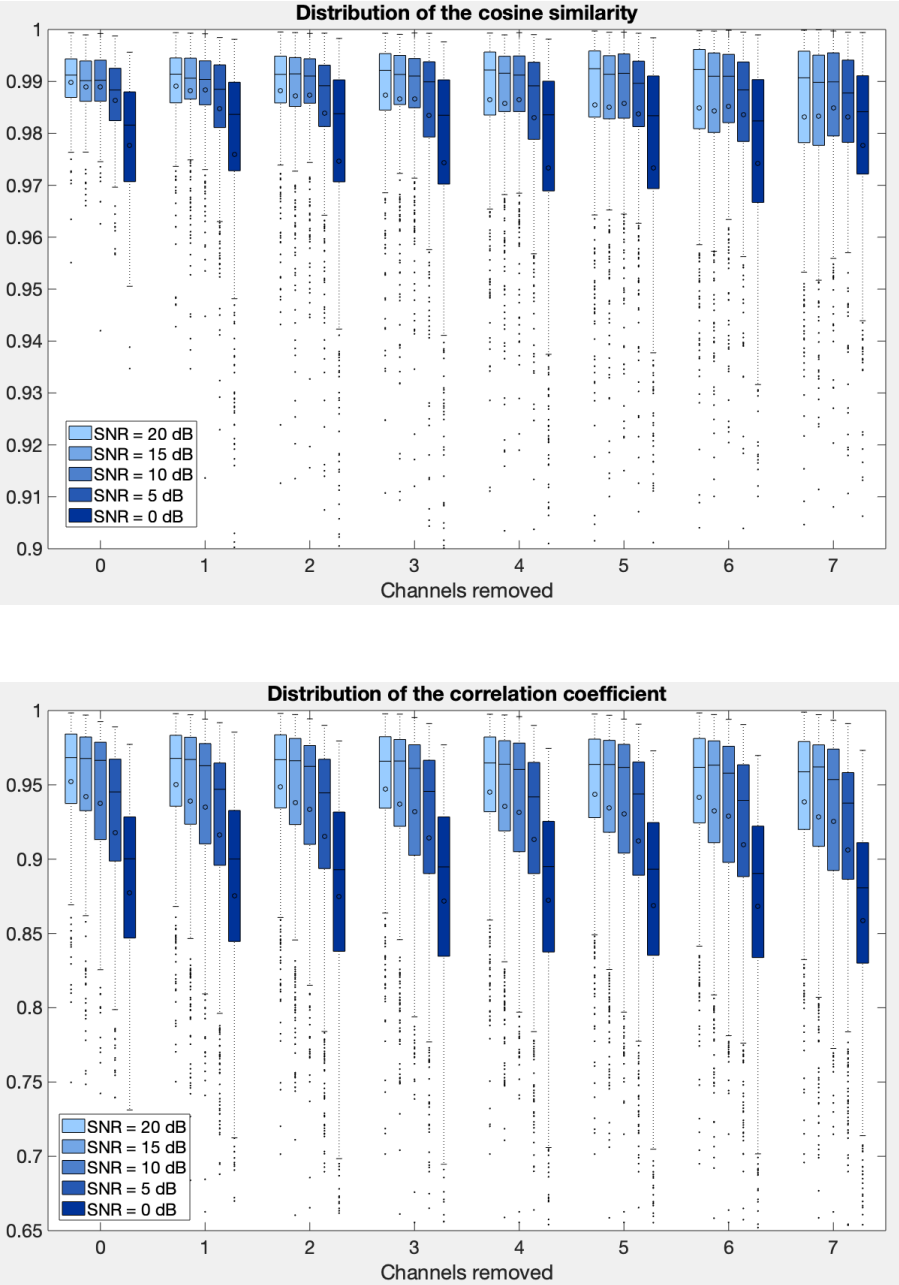

Figure 4.7: Distribution of the cosine similarity (up) and the correlation coefficient (down) between the synergies after the removal of channels and the original synergies as the number of removed channels increases: comparison for the different values of the SNR.

for the similarity) and not that far from the lower whiskers of the boxplots.

4.3 sEMG envelopes simulations starting from the synergies: shifting of the original envelopes

To observe how the algorithm reacts to the loss of channels, the cosine similarity and the correlation coefficient are computed after every removal between the new extracted synergies and the synergies that are reconstructed after having performed the shifting of the envelopes.

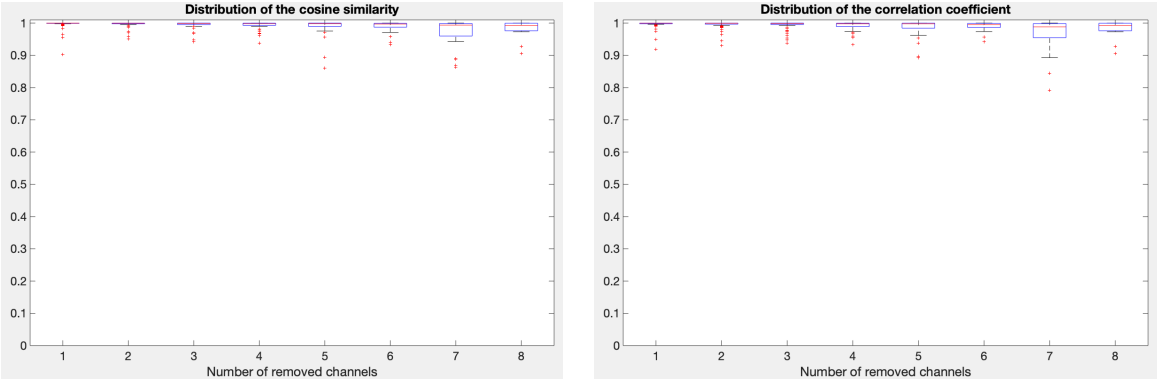

Figure 4.8: Distribution of the cosine similarity (left) and the correlation coefficient (right) between the synergies after the removal of channels and the original synergies as the number of removed channels increases - simulation with the shifted envelopes.

To observe how the shifting introduced in the envelopes affects reconstruction of the original signal through the NNMF as the number of channels decreases, the results for the cosine similarity and the correlation coefficient were computed (figures 4.8 and 4.9). In this simulation the number of synergies k is not fixed, but it is chosen (with the criteria described in section 3.4) in the first extraction of the synergies (from the original envelopes that have been shifted with the introduction of the parameter δ) and then it is kept for the following removal of the channels happening in that test. The natural ending of the simulation would be when the number of channels left is k+1 simulation is stopped when one synergy is lost, so when the synergies are computed with k-1 synergies. In the boxplots in the figures 4.8 and 4.9 the results are reported for the tests with the different k, so, for example, the last column reports the results when the channels lost are 8, but such a situation is possible only when the initial number of synergies is 3.
The performances of the algorithm are compared for the tests with different values of K in figure 4.11. The histogram in figure 4.10 reports the distribution of the number of simulations with a certain k (on the y axis there is the number of instances with respect to the total number of instances: this means that more or less

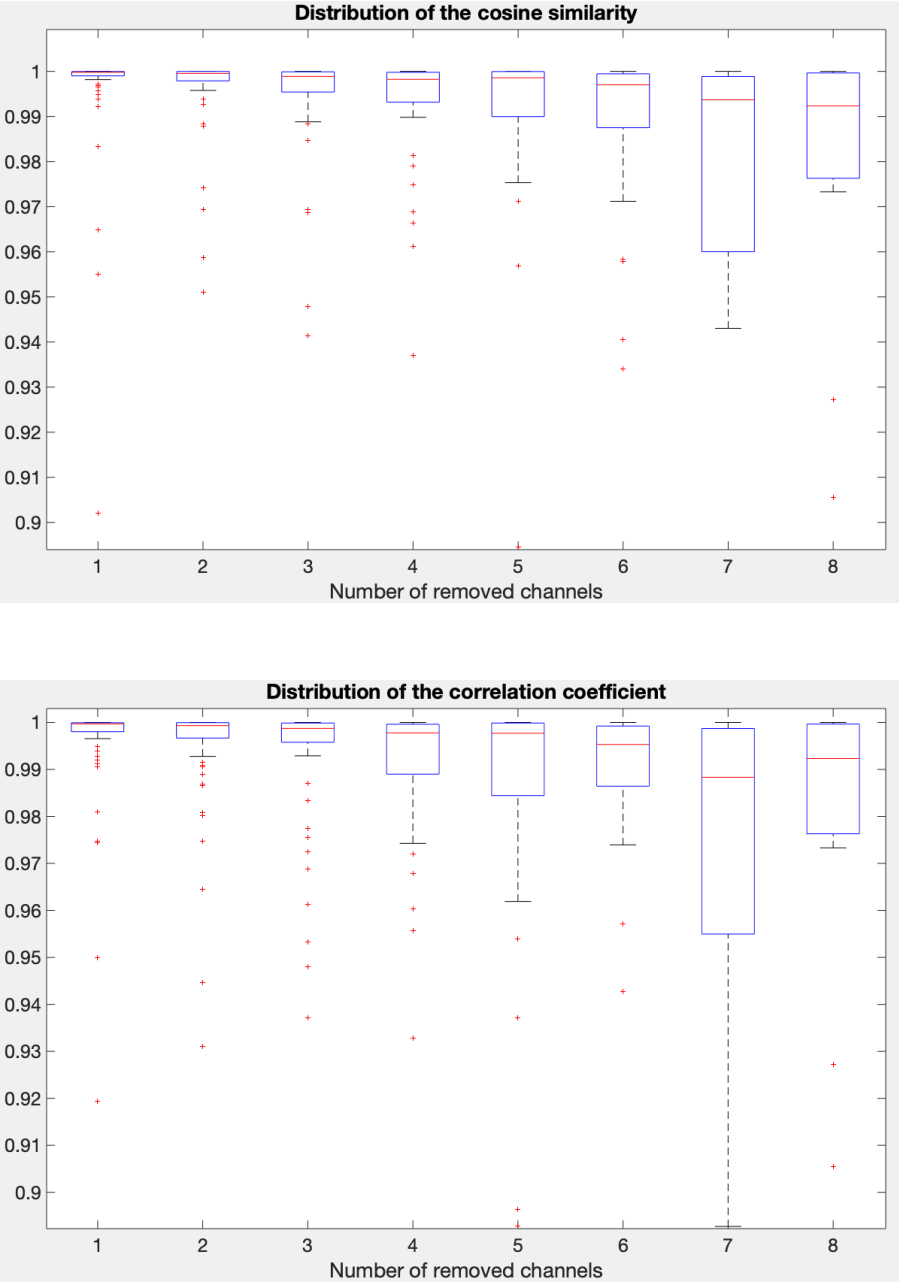

Figure 4.9: Distribution of the cosine similarity (up) and the correlation coefficient (down) between the synergies after the removal of channels and the original synergies as the number of removed channels increases - simulation with the shifted envelopes.

the 80% of tests has k=4 as initial number of synergies, the 15% of tests has k=3 and less than the 5% has k>4.

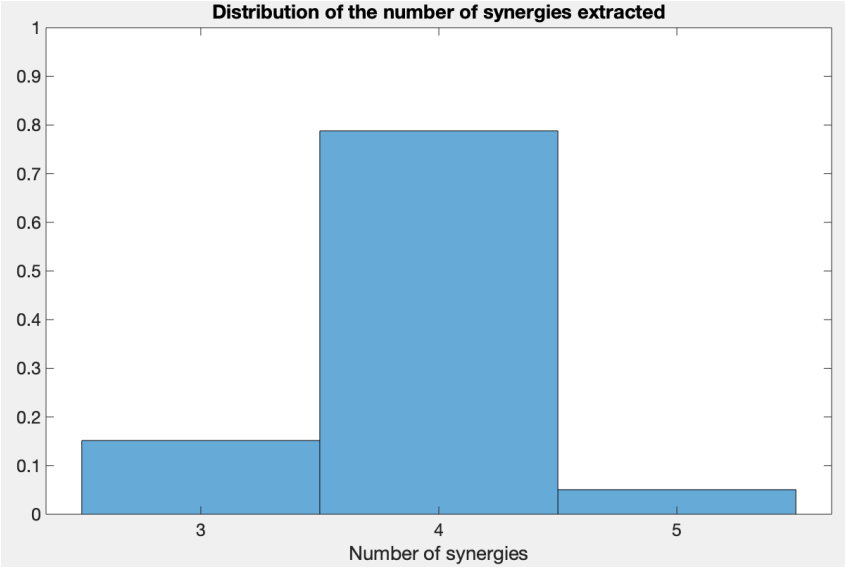

Figure 4.10: Distribution of the number of tests with a certain value of the starting number of synergies k.

In this simulation, if for the removal of one channel the number of synergies extracted (chosen according to the specific thresholds reported in 3.4) was smaller than the initial number of synergies, the test would stop, otherwise it would naturally end where the number of channels left would be equal to k+1. It is worth observing in how many instances the test is stopped before its ending and at what iteration. Observing the distributions of cosine similarity and cross correlation, it is noticeable that for k>4 the test is soon stopped, since only for 1 channel removed we have more than one instance, and from 4 channels removed on we do not have results. It was observed from the results that the tests with k=3 are never forcibly stopped, but the simulation is always performed until the end. For tests with k=4, in around 30% of the cases the simulation was performed until the end, in the remaining cases it stopped at the removal of a previous channel, with a even distribution of the instances that stopped at a certain number of channels.
Observing the comparison of the performances of the algorithm with k=4 and k=3 in figure 4.11 it is possible to notice that up until the 6th channel is removed the performances are really similar, only slightly better for k=3. The main difference is what happens when 7 channels are lost. This may be due to the fact that, if the NNMF has k=4 even with less channels, it will have more degree of freedom to explore to find the best reconstruction than the ones that it would have if k was equal to 3. Having more degrees of freedom, the algorithm, using k=4, might reach a solution for the extraction of synergies quite different from the original synergies

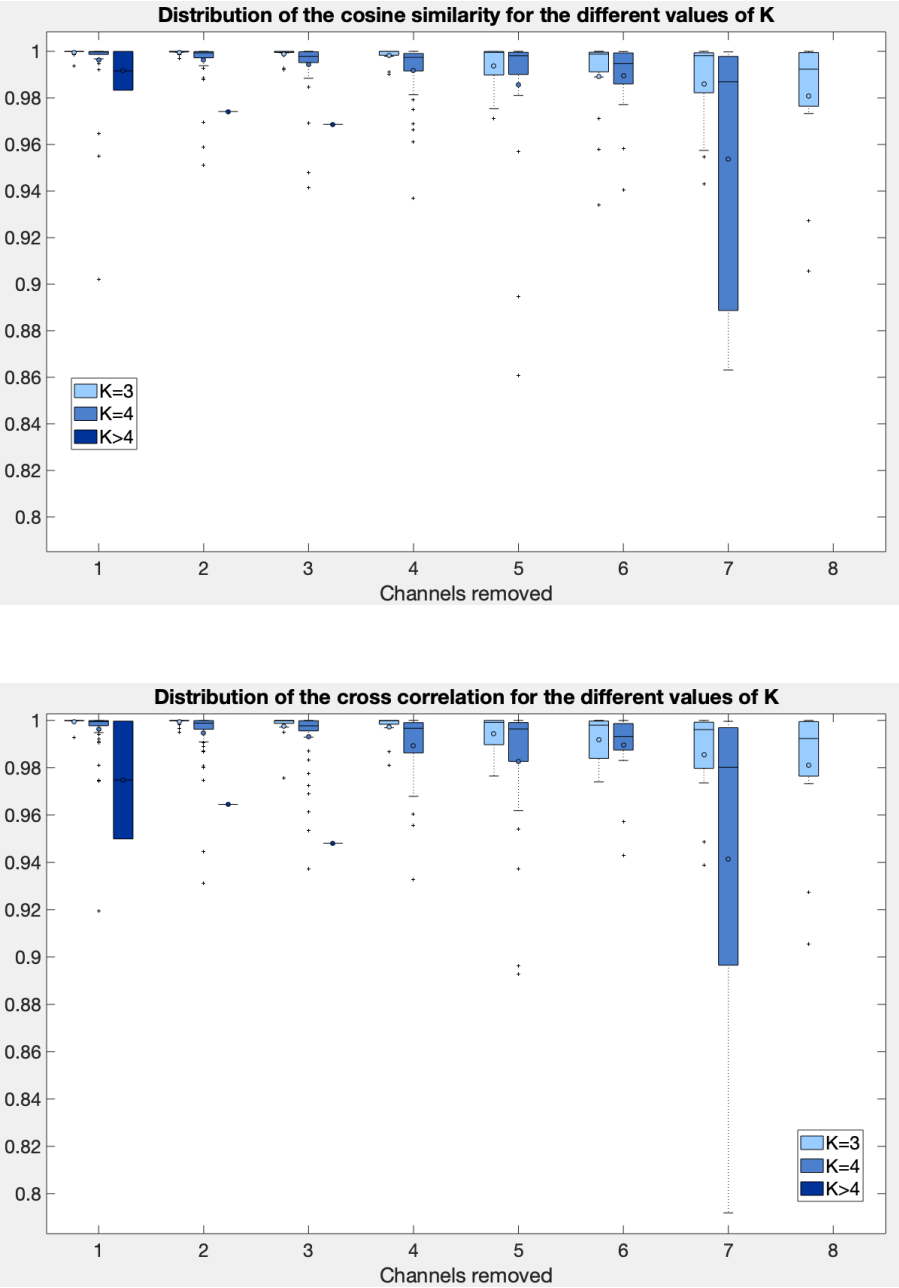

Figure 4.11: Distribution of the cosine similarity (up) and the correlation coefficient (down) between the synergies after the removal of channels and the original synergies:simulation with the shifted envelope, comparison of the results with the different values of k.

more easily than an algorithm with k=3 could. This is why, when the number of synergies is lower than the synergies obtained, they are often more similar to the

original synergies than when the number of synergies is higher. It is important to remember that, in most cases, the synergies obtained with an higher k are still valid and provide a good reconstruction of the signal, they are just different from the original ones.

4.4 sEMG simulations starting from physiological activations

The two simulations starting from physiological activations are performed (following the block diagram in figure 3.18) in a parallel way with two different constraints: in one, the channel that is removed is the best possible one, the channel for which the synergies extracted provided the best metrics for comparison with the original 5 synergies, the channel whose removal would less afflict the functioning of the algorithm. To simplify, this simulation will be called "Best" simulation. In the parallel simulation, the channel removed is the worst possible, the channel for which the synergies extracted provided the worst metrics for comparison with the original synergies, the channel whose removal would cause the performances of the algorithm to decrease the most. This simulation will be called "Worst" simulation. The results for these two simulations are presented at the same time.
In figure 4.12 is represented the variation of the Cosine Similarity (in red) and of the Correlation Coefficient (in blue) as the number of channels that are removed increases. The upper boundary of the coloured area represents the maximum value assumed by the parameter, the lower boundary the minimum value of assumed by the parameter and the center line represents the average value.

In the "Best" simulation, the values of Cosine Similarity and Correlation Coefficient remain more or less constant, and very close to 1, until we reach the removed channel number 10. At that point they start decreasing, but not so steeply, and even the minimum value that they reach (around 0.92 for the correlation and around 0.96) is still a really high value. The Correlation Coefficient is always slightly lower than the Cosine Similarity.
In the "Worst" simulation, the Correlation Coefficient decreases more rapidly than the Cosine Similarity until the removal of the 9th channel, then it is more or less stable with an average around 0.8. The Cosine Similarity is more or less stable until the same point, then oscillates, with its average oscillating in a range between 0.9 and 1, to reach the final value of 0.8. The average value of the Cosine Similarity is always greater than 0.8, but its minimum is highly variable and. in some instances, reaches values as low as 0.5, even 0.2 in the last step. On the other side,

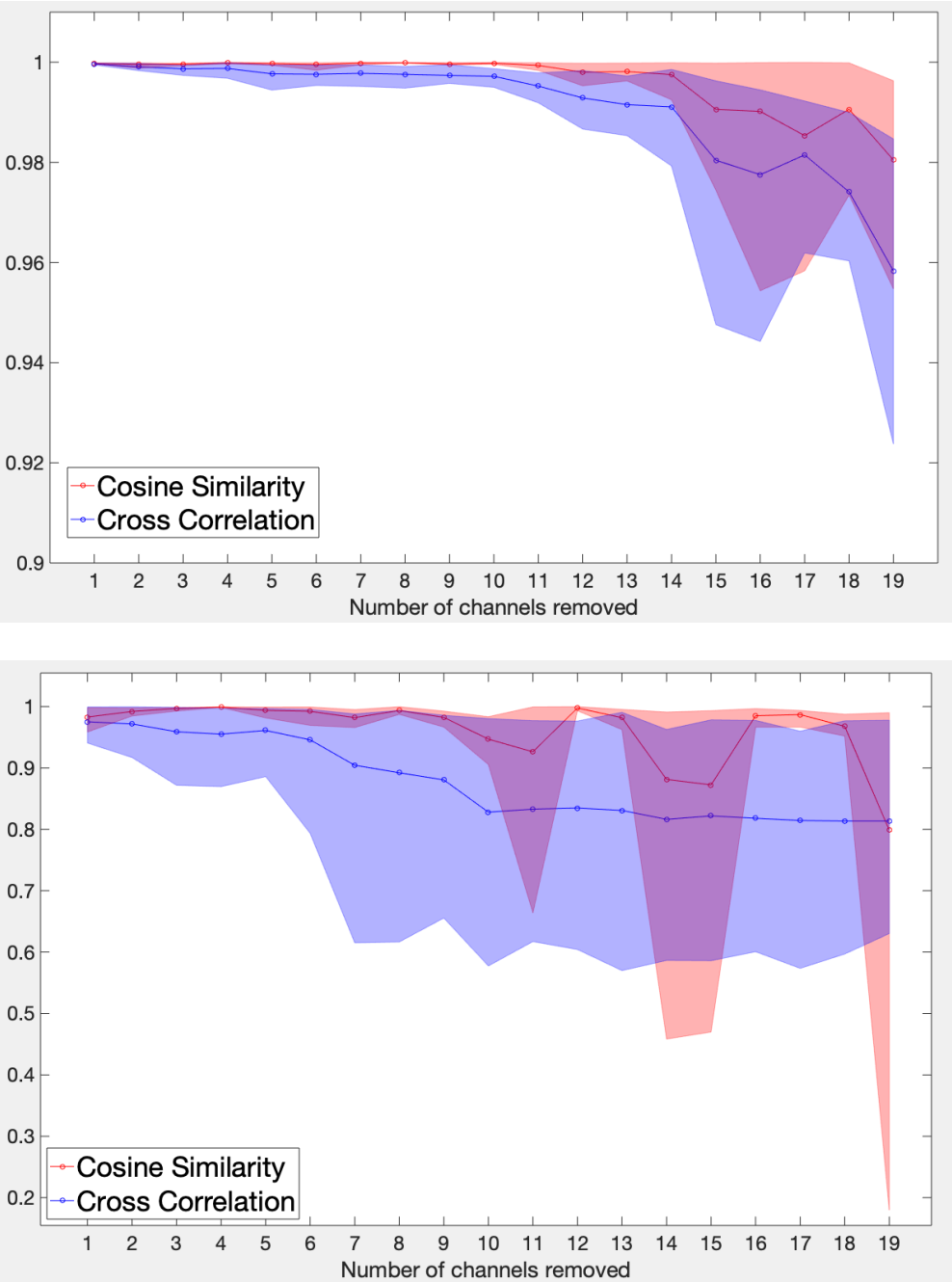

Figure 4.12: Trend of cosine similarity and correlation coefficient across the increasing of number of channels removed. Upper part of the figure: "Best" simulation. Lower part of the figure: "Worst" simulation. The center line represents the average of the parameter, while the lower and upper boundary of the colored area the minimum and maximum values.

the Correlation Coefficient is more stable and does not reach values as low.

We shall now analyze more in details what happens to the synergies as more and more channels are lost, and what can be observed on the channels lost. In figure 4.13 the synergies extracted when 5 channels had already been removed (the channels removed are indicated by a grey box) are reported. The channels that were lost, different for both simulations because of the opposite criterion by which they are selected, are:

	BEST SIM.			**WORST SIM.**	
Ch.	**Muscle**		**Ch.**	**Muscle**	
3	Biceps femoris	BF	1	Adductor longus	ADDL
4	Extensor digitorum longus	EDL	2	Adductor magnus	ADDM
11	External oblique lateralis	OEL	12	External oblique medialis	OEM
14	Peroneus longus	PERL	15	Rectus abdominus	RA
22	Tensor fascia latae	TFL	14	Splenius	SPLEN

Table 4.1: List of the first 5 muscles to be removed - best and worst simulation

The muscles lost in the "Best" simulation are muscles that are redundant for the extraction of the synergies, because some other muscle can give their same contribution to the computation of the synergies. For example, the External oblique lateralis OEL (channel 11) can be replaced by the External oblique medialis OEM (channel 12) and the Peroneus longus PERL (channel 14) can be replaced by the Peroneus brevis PERB (channel 13).
The muscles lost in the "Worst" simulation were probably muscles that have a peculiar activation that is not similar to other muscles, or that are very active in one or more synergies. This happens, for example, for the Adductor longus ADDL (channel 1), the External oblique medialis OEM (channel 12) and the Splenius SPLEN (channel 14): looking at their contribution to the original synergies obtained from the envelopes with all the channels (figure 3.17) it is possible to notice how the corresponding weight vectors for those muscles had an high value across multiple channels. Their loss is more problematic than the loss of the muscles from the "Best" simulation, since it may lead to the loss of some significant information that cannot be recovered. As it can be observed both visually comparing the synergies with the original ones and looking at the values of the metrics previously discussed,

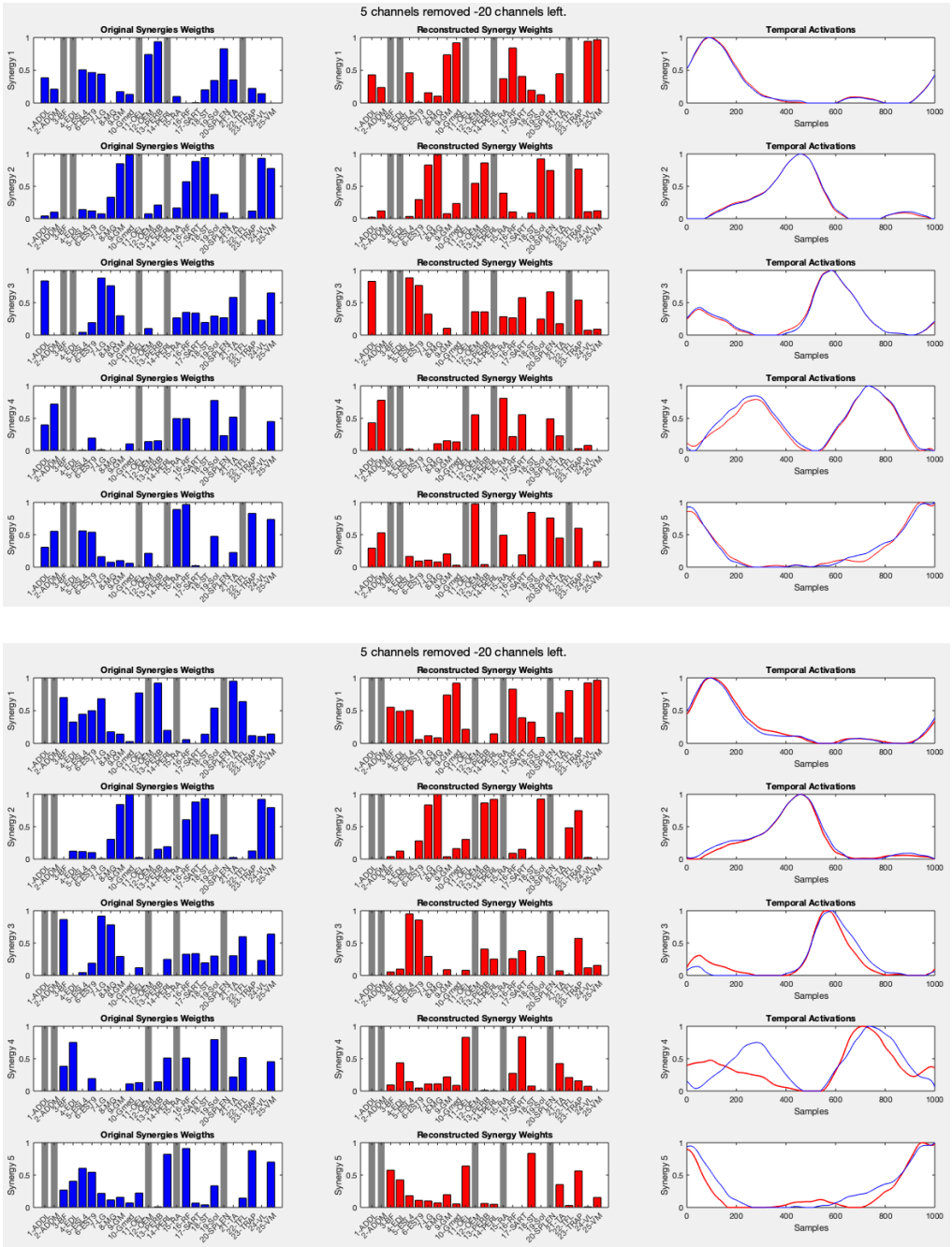

Figure 4.13: Synergies obtained when 5 channels have been removed compared with the original synergies with 25 channels. Upper part of the figure: "Best" simulation. Lower part of the figure: "Worst" simulation. In blue are represented the original synergies, in red the synergies after the removal of channels.

the reconstruction of the signal is still very good also with 5 channels less, and the extracted synergies are really similar to the original ones.

Figure 4.14 reports the synergies extracted when other 5 channels have been removed (total number of channels lost is 10). The channels that were lost, different for both simulations because of the opposite criterion by which they are selected, are:

	BEST SIM.			**WORST SIM.**	
Ch.	**Muscle**		**Ch.**	**Muscle**	
1	Adductor longus	ADDL	5	Erector spinae lumbar	ES(L4)
7	Gastrocnemius lateralis	LG	6	Erector spinae thoracic	ES(L4)
9	Gluteus maximus	GM	11	External oblique lateralis	OEL
12	External oblique medialis	OEM	17	Sartorius	SART
24	Vastus lateralis	VL	23	Trapezius	TRAP

Table 4.2: List of the second group of 5 muscles to be removed - best and worst simulation

Also in this case, some of the muscles lost in the "Best" simulation are still redundant muscles (for example the Peroneus longus PERL (channel 14) could be replaced by the Peroneus brevis PERB (channel 13) whose activation is really similar. For the worst simulation in this group of lost channels there are two that are redundant (Adductor longus ADDL and Adductor brevis ADDM, channels 1 and 2), but since they are lost almost at the same time the information linked to them cannot be recovered. Also at this point the reconstruction of the signal is still very good also with 5 channels less, and the extracted synergies are similar to the original ones.

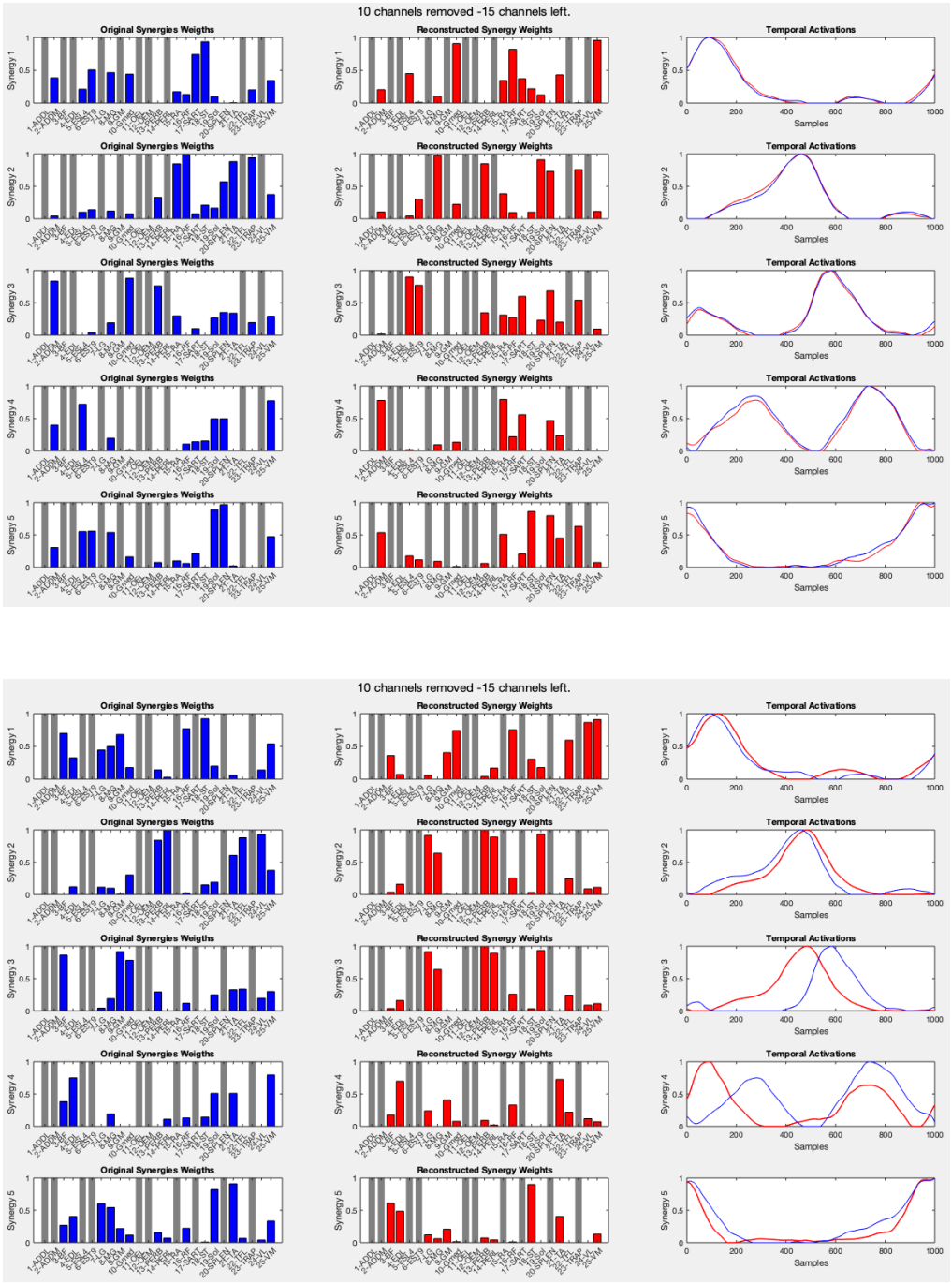

Figure 4.14: Synergies obtained when 10 channels have been removed compared with the original synergies with 25 channels. Upper part of the figure: "Best" simulation. Lower part of the figure: "Worst" simulation. In blue are represented the original synergies, in red the synergies after the removal of channels.

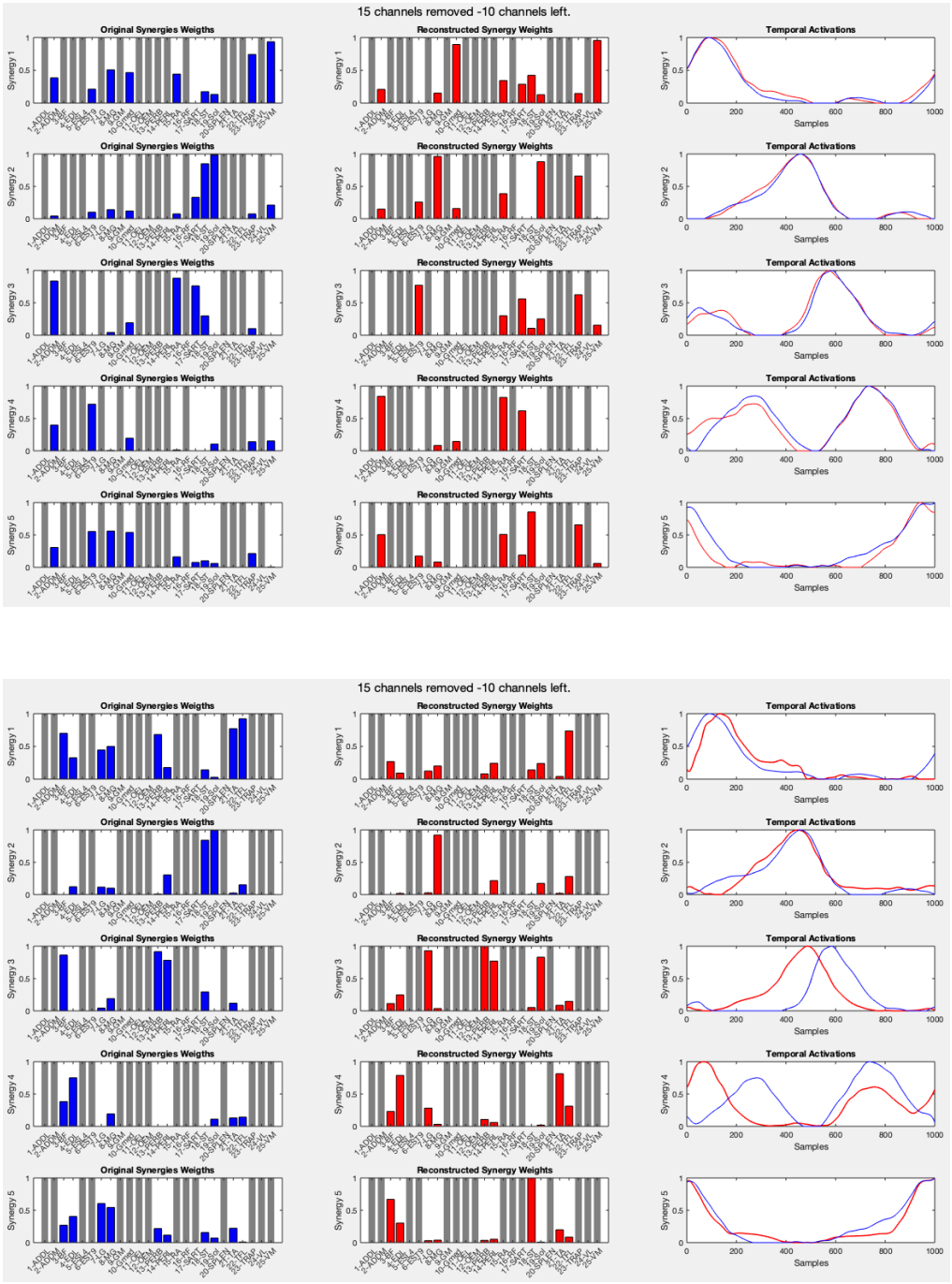

Figure 4.15: Synergies obtained when 15 channels have been removed compared with the original synergies with 25 channels. Upper part of the figure: "Best" simulation. Lower part of the figure: "Worst" simulation. In blue are represented the original synergies, in red the synergies after the removal of channels.

Figure 4.15 reports the synergies extracted when other 5 channels have been removed (total number of channels lost is 15). The channels that were lost are:

	BEST SIM.			**WORST SIM.**	
Ch.	**Muscle**		**Ch.**	**Muscle**	
5	Erector spinae lumbar	ES(L4)	9	Gluteus maximus	GM
13	Peroneus brevis	PERB	10	Gluteus Medius	Gmed
16	Rectus femoris	RF	16	Rectus femoris	RF
20	Splenius	SPLEN	24	Vastus lateralis	VL
21	Tibialis anterior	TA	25	Fifth metatarso-phalangeal joint	VM

Table 4.3: List of the third group of 5 muscles to be removed - best and worst simulation

At this point, with so many channels removed,it is difficult to make considerations on the channels that have been removed within this group. Looking at the previous graph, it can be noticed that this is the moment when the Cosine Similarity and Correlation Coefficient start dropping, but their absolute values are still good.
The last bunch of channels removed in figure 4.16 consisted of:

	BEST SIM.			**WORST SIM.**	
Ch.	**Muscle**		**Ch.**	**Muscle**	
2	Adductor magnus	ADDM	4	Extensor digitorum longus	ES(L4)
19	Soleus	Sol	18	Semitendinosus	ST
23	Trapezius	TRAP	19	Soleus	Sol
25	Fifth metatarso-phalangeal joint	VM	22	Tensor fascia latae	TFL

Table 4.4: List of the last group of 4 muscles to be removed - best and worst simulation

Since this is the last group of channels that was removed, it makes more sense to look directly at the 6 channels that remain both for the "Best" and "Worst" simulation.

	BEST SIM.			**WORST SIM.**	
Ch	**Muscle**		**Ch**	**Muscle**	
6	Erector spinae thoracic	ES(T9)	3	Biceps femoris	BF
8	Gastrocnemius medialis	MG	7	Gastrocnemius lateralis	LG
10	Gluteus medius	Gmed	8	Gastrocnemius medialis	MG
15	Rectus abdominus	RA	13	Peroneus brevis	PERB
17	Sartorius	SART	14	Peroneus longus	PERL
18	Semitendinosus	ST	21	Tibialis anterior	TA

Table 4.5: List of the 6 muscles that are left after 19 channels are removed - best and worst simulation

As far as the "Best" simulation is concerned, it is not appropriate to assume that the channels left behind are the absolute best, able to perfectly reconstruct the synergies. This process of choice of the best channels often discriminates between values of the metrics that are really close, so at any point another channel could have been picked and still be valid and the final solution could have been completely different. It would be necessary to perform the same test many times and individuate the channels that were left as last channels more frequently. Moreover, it is reasonable to think that the channels left are simply channels whose temporal activation is similar to the temporal activation of the original synergies.
For what concerns the "Worst" simulation, it is remarkable how 4 out of the 6 channels left consist of two couples of redundant channels (Gastrocnemius lateralis and Gastrocnemius medialis; Peroneus brevis and Peroneus anterior): it is pointless to keep both channels from these couples because they give the same information and other channels potentially more informative could have been more useful, so it makes sense that they were picked as worst channels.

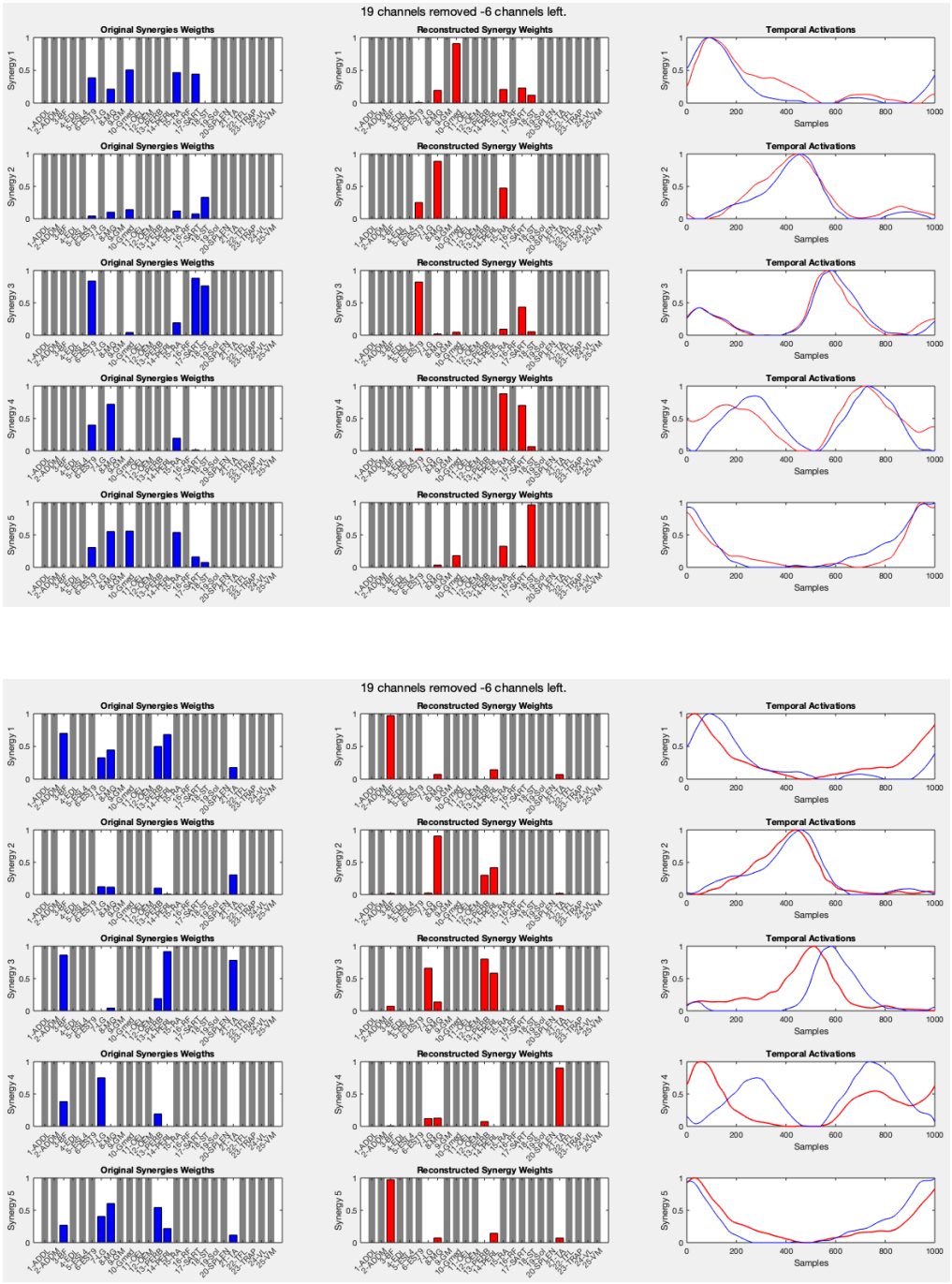

Figure 4.16: Synergies obtained when 19 channels have been removed compared with the original synergies with 25 channels. Upper part of the figure: "Best" simulation. Lower part of the figure: "Worst" simulation. In blue are represented the original synergies, in red the synergies after the removal of channels.

Chapter 5

Conclusions

The aim of this thesis was analyzing the changes in the final factorization performed by the NNMF algorithm when one or more input channels are removed, evaluating the performances by computing metrics on the synergies. The first set of simulation performed had as starting point four generated activations: keeping the number of synergies fixed to k=4, a very good reconstruction was obtained even when many channels were removed. In some cases there was a drastic decrease in the similarity of the new synergies with respect to the initial ones. This indicates the presence of outliers, than can be divided into three categories:

- one of the synergies is almost lost (the corresponding weight vector has a norm close to 0)
- one of the synergies after the removal of channels can be considered as merging of some of the original synergies
- two or more of the synergies after the removal of channels can be explained as a fractionation of one of the original synergies

These three categories cover a good part of all the outliers.

The previous condition was not realistic one, because the algorithm had to perform a perfect factorization, while in real applications the algorithm is always faced with a pseudo factorization. Some variability in the signals was then induced.

In a second simulation the Signal to Noise ratio was added to the picture, analyzing how the NNMF performs when dealing with sEMG signals. It has been observed that an increase of the SNR leads to a decrease of the similarity.

In the third simulation, a parameter acting as a jitter was added to the simulated activations, to introduce some variability. To take into account this variability the number of synergies to be extracted was no longer fixed to k=4, but it was left free to change only considering some constraints on the quality of the reconstruction.

The introduction of the jitter reduces the number of the outliers. In fact, the fact that the algorithm is now performing a pseudo factorization and not an exact one makes it harder to reconstruct the same synergies in different ways. Leaving to the algorithm the choice of the number of synergies to compute also leads to the absence of merging and fractionation.

In this simulation, a stop condition was set for the algorithm when one synergy was lost before reaching the ideal ending of the simulation, that should happen when the number of channels is equal to k+1. In the tests where k was equal to 3, k remained always the same and the ideal ending was always reached, while in the tests with k=4 the simulation was stopped before the ending because the number of synergies had decreased in the 65% of the cases.

This simulation had a really low number of outliers: this suggests that the reason for the outliers in the first simulation might have been the fact that the algorithm was left with too many degrees of freedom, so it was more probable for it to converge to a solution in a different portion of the space of the solutions and so different from the original one.

As a final step, simulations with signals taken from a real application were performed. The data were obtained digitizing some activations of muscles involved in gait, presented by Ivanenko [28]. Starting from 25 channels, two parallel simulations were performed: in the first one the channel that is removed was the one from whose synergies the highest metrics of comparison with the original synergies were obtained ("best simulation"), in the second one the channel with the lowest metrics is removed ("worst simulation"). The number of synergies was fixed to k=5 and the removal of channels continued until 6 channels were left.

The algorithm could reconstruct well the signals even when losing a lot of channels in both cases. This approach could be used to identify subsets of channels that could easily be removed without affecting much the reconstruction, or on the other end subsets of channels whose loss could badly affect the reconstruction.
Considering the last channels that are left after all the removals, in the "worst"

simulation they were redundant channels as it was expected. Considering only this simulation it would be wrong to infer that the channels that remained at the end of the "best" simulation were perfectly able to reconstruct the initial signal, it is more probable that the channels left have simply an high correlation with the temporal activation of the initial synergies. With a longer and more robust simulation it could be possible to identify an ideal set of muscles that could reconstruct the original synergies to use them to reconstruct the signal of a missing channel.

Acknowledgements

I would like to thank Prof. Paolo Bonato for having me in his laboratory, for his patience and for guiding me with his knowledge.

Living this experience would not have been possible without the supervision of Prof. Gabriella Olmo, i will always be grateful to her for giving me this great opportunity.

I would like to express my most sincere gratitude to Dr. Stefano Sapienza, for patiently answering all my questions and doubts, for teaching me a lot and for encouraging me when i needed it.

Big thanks also to all the members of the Motion Analysis Laboratory to have make this experience unforgettable, especially to the fellow master students Monica, Federica and Giovanni who have been my family in Boston.

I would like to thank all my friends, i always felt their support in everything i do despite the distance and even if we are now spread through the world i know i can count on you. It would be too long to list all of them, but i can't not say a special thanks to Chiara, Fausto and Francesca who have always listened to all my problems helping me to find solutions.

Finally, i would like to thank my father Gianfranco, my mother Orsolina and my sister Monica, for having always believed in me and in my dreams, helping in achieving them, and for showing me their love everyday.

Acronyms

AP Action Potential.

CNS Central Nervous System.

DoF Degrees of Freedom.

EMG ElectroMyoGraphy.

FA Factor Analysis.

ICA Independent Component Analysis.

iEMG Intramuscular ElectroMyoGraphy.

MU Motor Unit.

MUAP Motor Unit Action Potential.

NNMF Non-Negative Matrix Factorization.

PCA Principal Component Analysis.

PLI Power Line Interference.

SCI Spinal Cord Injuries.

sEMG Surface ElectroMyoGraphy.

VAF Variance Accounted For.

Bibliography

[1] E. J. J. E. J. O. K. D. H. K. B. P. J. A. W. M. W. J. Gordon Betts, Peter DeSaix and K. A. Young, "Anatomy & physiology," pp. 160– 161, Openstax, 2013.

[2] E. J. J. E. J. O. K. D. H. K. B. P. J. A. W. M. W. J. Gordon Betts, Peter DeSaix and K. A. Young, "Anatomy & physiology," pp. 407–420, Openstax, 2013.

[3] J. E. Hall, "Guyton and hall textbook of medical physiology (12th edition)," pp. 79–91, Elsevier Health Sciences, 2020.

[4] J. L. N. Frederic H. Martini, Robert B. Tallitsch, "Human anatomy (ninth edition)," pp. 236–255, Pearson, 2018.

[5]

[6] "Analysis of intramuscular electromyogram signals," vol. 367, p. 357, 2009.

[7] W. R. G. L. N. S. De Luca CJ, Adam A, "Decomposition of surface emg signals," vol. 96, p. 1646, 2006.

[8] V. T. Cavalcanti Garcia MA, "Surface electromyography: Why, when and how to use it," vol. 4, pp. 17–28, Elsevier, 2011.

[9] Carlo J. De Luca, *SURFACE ELECTROMYOGRAPHY: DETECTION AND RECORDING*, 2002. https://www.delsys.com/downloads/TUTORIAL/semg-detection-and-recording.pdf.

[10] M. C. C. A. F. L. E. B. E. A. d. D. Torricelli, F. Barroso, "Muscle synergies in clinical practive: Theoretical and practical implications," pp. 251–272, 2016.

[11] A. M. S. S. B. C. K. P. P. S. B. P. B. E. Cheung VC, Turolla A, "Muscle synergy patterns as physiological markers of motor cortical damage.," vol. 109, pp. 14652–14656, Sep 2012.

[12] M. Castagna, "Feasibility study of average threshold crossing (atc) technique application in muscle synergies analysis.," 2019.

[13] "Major muscles on the front of the body," 2020. [Online; accessed 20-September-2020].

[14] W. DA, "The biomechanics and motor control of human gait: Normal, elderly and pathological," Waterloo Biomechanics Press, 1991.

[15] J. E. Hall, "Guyton and hall textbook of medical physiology (12th edition)," p. 127, Elsevier Health Sciences, 2020.

[16] W. R. Frontera and J. Ochala, "Skeletal muscle: A brief review of structure and function," *Calcified Tissue International*, vol. 96, no. 3, pp. 183–195, 2015.

[17] G. e. a. Anastasti, "Trattato di anatomia umana, vol 1 (4 edizione)," pp. 75–84, Edi Ermes, 2010.

[18] Wikipedia contributors, "Electromyography Wikipedia, the free encyclopedia," 2020. [Online; accessed 10-September-2020].

[19] M.-Y. F. Reaz MBI, Hussain MS, "Techniques of emg signal analysis: detection, processing, classification and applications," vol. 8, pp. 11–35, 2006.

[20] B. N, "The coordination and regulation of movements," 1967.

[21] B. E. Cheung VC, "The neural origin of muscle synergies," vol. 7, 2013.

[22] d. A. S. P. T. M. Bizzi E, Cheung VC, "Combining modules for movement," vol. 57, pp. 123–133, 2008.

[23] B. E. Tresch M, Saltiel P, "The construction of movement by the spinal cord," vol. 2, pp. 162–167, 1999.

[24] d. A. T. M. B. E. Saltiel P, Wyler-Duda K, "Muscle synergies encoded within the spinal cord: evidence from local intraspinal nmda iontophoresis in the frog," vol. 85, pp. 605–619, 2001.

[25] L. M. A and G. W. M, "Modularity of motor output evoked by intraspinal microstimulation in cats," vol. 91, pp. 502–514, 2004.

[26] B. E. Tresch M, "Responses to spinal microstimulation in the chronically spinalized rat and their relationship to spinal systems activated by low threshold cutaneous stimulation," vol. 129, pp. 401–416, 1999.

[27] T. L. H. Torres-Oviedo G, "Muscle synergies characterizing human postural responses," vol. 98, pp. 2144–2156, 2007.

[28] L. F. Ivanenko Y P, Poppele R E, "Five basic muscle attivation patterns account for activity during human locomotion," vol. 556, pp. 267–282, 2004.

[29] P. R. E. L. F. Cappellini G, Ivanenko Y P, "Motor patterns in human walking and running," vol. 95, pp. 3426–3437, 2006.

[30] "Consistency of muscle synergies during pedaling across different mechanical constraints," vol. 106, pp. 91–103, 2011.

[31] "Modulation of phasic and tonic muscle synergies with reaching direction and speed," vol. 100, pp. 1433–1545, 2008.

[32] "Muscular and postural synergies of the human hand," vol. 92, pp. 523– 535, 2004.

[33] "Effective force control by muscle synergies," vol. 8, pp. 1–12, 2014.

[34] "Temporal components of the motor patterns expressed by the human spinal cord reflect foot kinematics," vol. 90, pp. 3555–3565, 2003.

[35] "Distributed neural networks for controlling human locomotion. lessons from normal and sci subjects," vol. 78, pp. 13–21, 2009.

[36] "Impulses of activation but not motor modules are preserved in the locomotion of subacute stroke patients," vol. 106, pp. 202–210, 2011.

[37] "Matrix factorization algorithms for the identification of muscle synergies: Evaluation on simulated and experimental data sets," vol. 95, pp. 2199–2212, 2006.

[38] "Algorithms for non-negative matrix factorization," pp. 535–541, 2000.

[39] M. Grimaldi, "Machine learning techniques for movement recognition in wearable technology applications for rehabilitation," 2017.

[40] "Non-negative matrix factorization algorithms modeling noise distributions within the exponential family," pp. 535–541, 2005.

[41] "Learning the parts of objects by non-negative matrix factorization," vol. 401, pp. 788–791, 1999.

[42] "Decomposing time series data by a non-negative matrix factorization algorithm with temporally constrained coefficients," pp. 3496–3499, 2015.

[43] "Combinations of muscle synergies in the construction of a natural motor behavior," vol. 6, pp. 300–308, 2003.

[44] P. P. Merletti R, "Electromyography: physiology, engineering and non-invasive applications," John Wiley Sons, 2004.

[45] MATLAB, *version 9.7.0.1261785 (R2019b)*. Natick, Massachusetts: The MathWorks Inc., 2019.

[46] Wikipedia contributors, "Coefficient of determination r2 Wikipedia, the free encyclopedia," 2020. [Online; accessed 10-August-2020].

[47] T. L. Torres-Oviedo G, Macpherson JM, "Muscle synergies organization is robust across a variety of postural perturbations," vol. 96, pp. 1530–1546, 2006.

[48] Jan-Willem van Wingdern, TU Delft Center for System and Control, "Vaf," 2020. [Online; accessed 10-August-2020].

[49] R. D, V. Agostini, and M. Knaflitz, "Intra-subject consistency during locomotion: Similarity in shared and subject-specific muscle synergies," vol. 11, 2017.

[50] "The number and choice of muscles impact the results of muscle synergy analyses," vol. 7, pp. 1–16, 2013.

[51] "Frequency parameters of the myoelectric signal as a measure of muscle conduction velocity," vol. 8, pp. 515–523, 1981.